1-1-2012

Novel Biodegradable Polyurethanes Reinforced With Green Nanofibers for Applications in Tissue Engineering

Hamza M. Nakhoda
Ryerson University

NOVEL BIODEGRADABLE POLYURETHANES REINFORCED WITH GREEN NANOFIBERS FOR APPLICATIONS IN TISSUE ENGINEERING

by

HAMZA M. NAKHODA

B.S. Biomedical Engineering

University of Southern California, Los Angeles, 2010

A thesis presented

to Ryerson University

in partial fulfillment of the

requirements for the degree of

Master of Applied Science

in the Program of

Chemical Engineering

Toronto, Ontario, Canada, 2012

AUTHOR'S DECLARATION

I hereby declare that I am the sole author of this thesis. This is a true copy of the thesis, including any required final revisions, as accepted by my examiners.

I authorize Ryerson University to lend this thesis to other institutions or individuals for the purpose of scholarly research.

I further authorize Ryerson University to reproduce this thesis by photocopying or by other means, in total or in part, at the request of other institutions or individuals for the purpose of scholarly research.

I understand that my thesis may be made electronically available to the public.

ABSTRACT

New class of green biocomposites were designed and synthesized for tissue engineering applications. These newly introduced non-cytotoxic, biodegradable polyurethane composites had different compositions (i.e., ratio of hard to soft segments) of the linear, aliphatic hexamethylene diisocyanate and polycaprolactone diol. The porosity was introduced in the polyurethane matrix using a combination of salt leaching and thermally induced phase separation (TIPS). The resulting interconnected pore size was characterized using Scanning Electron Microscope (SEM) to be between 125-355 μm. Porosity was determined using liquid displacement and found to be between 70-75% for non-reinforced matrices, 64-70% for reinforcement with 5 wt% biocellulose nanofiber (BCNF), 59-69% for 10 wt% BCNF, and 57-69% for 15 wt% BCNF biocomposite samples. Dependent on the composition, compressive strength showed up to a little less than two-fold increase (85%) for green BCNF reinforcement of 5 wt% and more than two-fold increase (120%) for 10 wt%. The tensile strength also increased up to almost two-fold (114%) for reinforcement with 5 wt% BCNF and to more than two-fold (140%) for 10 wt% reinforcement. Higher degrees of reinforcement showed a detrimental effect on both properties. Properties demonstrate that this novel class of nanostructured biocomposite holds potential to be utilized as scaffolds for tissue regeneration.

ACKNOWLEDGEMENTS

First and foremost, I would like to express my sincere gratitude to my supervisor, Dr. Yaser Dahman, who has supported me throughout my thesis with his patience and knowledge whilst allowing me the room to work in my own way. He has been a great mentor and without him this thesis would not have been completed or written. One simply could not wish for a better or friendlier supervisor. He has been a great source of inspiration and motivation for me and he always made it a point to keep me on my toes.

I also thank both Dr. Jiangning Wu and Dr. Simant Upreti for being part of my thesis committee and for providing invaluable feedback to this work. Other professors at Ryerson have also helped towards achieving my goals of a master's degree. I thank the academic and financial support received from the Department of Chemical Engineering at Ryerson University.

I would also like to thank my colleagues in the graduate program, including but not limited to Kashif Syed, Wahib Al-Abdallah, Banafsheh Mohtasebi, Hameed Muhammad, Shahzad Baig, Chumangalah Thirmal, Vishal Patel, Charles Ugwu, Ciro LeCompte, and last but not least Adriana Gaona. They gave me the strength to plod on despite my constitution wanting me to give up and throw in the towel. Throughout my life I have been blessed with the support of family, friends, teachers, advisors and well-wishers to pursue and eventually complete my masters degree. My friends Leena Sorathia, Owaiz Haji, Asadali and Shaikha Matcheswalla, Jared Ali, Amrita Arora, Ahmed Omar, Lavanya Venkat, Natalia Dhirani, and many others gave me a much needed outlet from research and studies during this academic venture.

Further I would like to thank Alan Machin for help with the mechanical testing, Ali Hemmati and Daniel Boothe for all the technical assistance including making the molds. I would like to thank Dr. Russell Viirre from the Department of Chemistry at Ryerson University, for allowing me to conduct NMR analyses. Many thanks to the help received from Mr. Qiang Li, from the Department of Mechanical Engineering at Ryerson University, who conducted SEM analyses. I would also like to acknowledge Shawn McFadden for his support with the FTIR equipment.

Finally, I wish to thank my family for their unconditional love and support. Also my most important role models, my mom Dr. Tasneem and my dad Mikhdad, who have supported me in every single stage of my life, giving me the opportunities to reach this level of education and filling my life with joy. They provided me with monetary provisions and a home to complete my write-up. I would particularly like to mention the Nakhoda, Karachiwala, and Cassoobhai families who stood by me. My most sincere gratitude and appreciation to my sister Azeemah, grandparents (Nizar, Mustaaly, Tehmina, and Sehra), cousins (Sultan, Samira, Mehreen, Alyna, Aadil, Shehzaad, Riaz, Shahnawaz, Shazia, Tasneem, Zahra, and Talib), uncles (Aameer, GulamHussein, Abazer, Zoheir, and Munawarali), aunts (Ferhana, Zainab, Qureisha, Mariyah, and Adiba), and nieces (Suroor, Sarah, Sakina, and Zahra). Their understanding and fortitude during this demanding journey is greatly appreciated. I also offer regards and greetings to all those who supported me in any way during the completion of this work and whose names were not mentioned

Dedicated to my parents, and sister, and also to all the researchers who strive to scratch their names in the world of tomorrow

TABLE OF CONTENTS

Page

LIST OF TABLES

Page

LIST OF FIGURES

Page

CHAPTER 1

INTRODUCTION

The utopian quest for immortality has been in the minds of philosophers and idealists long before our time. In the more practical world of science we settle for longer, enhanced quality of lives, which creates a conducive atmosphere for products that improve, safeguard, and restore our bodies. The vast majority of the field of tissue engineering deals with ways to replace damaged organs, tissues, or even cells so that they can gain back their original functionality, fully or in part.

A large part of our motor functions are controlled by the skeletal system and understandably a significant amount of resources are dedicated to research in the field of bone regenerative medicine. Scaffolds are a chief part of biomaterial science and are used as biodegradable implants that are capable of supporting the host tissue, guiding the tissue to grow within it and degrading in the body as the tissue regenerates.

Polymers are at the forefront of scaffold application as their properties are easier to manipulate. From controlling hydrophobicity to strength they can be a chemist's tools for substituting various tissues in the body. Polyurethane, in particular, attracts immense curiosity as it can be engineered from an array of hard and soft domains and the ratios of these domains can be altered to synthesize idiosyncratic materials. Usually, the soft segment is thought to comprise the hydrophobic, flexible structure and the hard segment, the more rigid, hydrophilic part. The latter can be in either aliphatic or aromatic form and the aliphatic is seen to have less cytotoxic, carcinogenic, and mutagenic biodegraded

products (Szycher et al., 1991). The diisocyanate hard segment chosen in this study was the linear hexamethylene diisocyanate (HDI) that is seen to react well with polycaprolactone diol (PCL) to synthesize original polymers that are biodegradable. Upon degradation, this novel composition that utilizes the linear HDI should yield l-lactic acid, hydroxy-hexanoic acid, hexanediamine and butanediol, which were found to be non-toxic in low concentrations as degradation products of nerve guides (Den Dunnen et al., 1993). These custom tailored, segmented polyurethanes have excellent mechanical properties, blood and tissue compatibility, in addition to biodegradability that is determined by the structural composition of the polymer (Gunatillake et al., 2006).

Scaffolds in tissue engineering require interconnected porosity due to an assortment of incentives. Cells can attach within this scaffold, ingrowth of tissue is viable, nutrients and waste can transport through the matrix, and consequently bulk biodegradability can be controlled based on the pores (Porter et al., 2009). However, the porosity is detrimental to the mechanical properties of the implant and reinforcement is needed to diminish this effect. Nano-scale materials can be used to combine with and support the structure of the scaffold and compensate for the loss in strength caused by the porous structure in scaffolds. Biocellulose nanofibers show impressive biocompatibility and physical properties (Sani and Dahman, 2009). Their extraordinary purity, crystallinity, optical transparency, and ductility have made them viable in state of the art applications in the medical and biotechnology fields. Recently, these nanofibers were synthesized from renewable resources like agriculture wastes (Dahman et al., 2010). Studies have shown that adding these green nanofibers to wide range of polymer matrices can enhance their strength, although may lower their porosity with the 3-D matrix (Xu et

al., 2001). By tailoring the final composition (ratio of hard to soft segments and the percentages of reinforced nanofibers), the resulting green biocomposites can thus be designed to mimic the mechanical properties of specific tissues. This can be further utilized to repair and regenerate a collection of vast range of specialized tissues.

The main objective of the present work is to design and synthesize novel green class of biocomposites for applications in regenerative medicine. The novel biocomposites will mainly be a continuous matrix of polyurethane with novel composition of hard and soft segment. This linear (or aliphatic) HDI will reduce the cytotoxicity and improve the biodegradation compared to the commonly utilized aromatic segments such as 4,4'-Diphenylmethane isocyanate (MDI) and 2,4-toluene diisocyanate (TDI) (Cardy and others, 1979). Final product is a porous scaffold that has the capability and structural integrity to mimic different bone tissues. Several polyurethane compositions with different ratios of hard to soft segments will be synthesized and examined to account for wider range of bone tissue regeneration applications. Green biocellulose nanofibers produced from renewable resources will be used as reinforcing element to compensate for the loss in mechanical properties due to the porous structure of the scaffold.

Manipulating the ratios of the hard and soft segment (i.e. NCO and OH content or HDI:PCL) can be justified by observing the functionality and composition of the synthesized blends. Furthermore, polyurethane needs to be made into scaffolds by inducing porosity, which is consequently measured, and the pore morphology that is visualized. The effect of adding reinforcement and increasing the content of that reinforcement is also of vital interest. For every scaffold prototype, the tensile and

compressive strengths are determined to give a better understanding of the physical characteristics of the matrix. The applicability of this promising biocomposite with a wide range of properties such as repairing and regenerating different tissues in the body needs to be ascertained. Biodegradability and other specific properties are also altered and can be controlled due to this manipulation.

CHAPTER 2

LITERATURE REVIEW

2.1 Bone Regeneration Studies

Bones form the basis of the musculoskeletal system. There are more than 200 bones in the adult human body, ranging from different shapes, sizes, and more importantly their mechanical properties. From the large tibial and femoral bones to the tiny stapes in the ear, the load-bearing role lies within a large array. Their function of supporting and protecting the various organs in the body make them vital structures. The human body can suffer accidents that induce trauma, injuries, and degenerative diseases, such as, arthritis and tumors. In most of these cases, the bone does not rejuvenate by itself and would need facilitation to be replaced. Therefore, a lot of emphasis is placed on the reconstruction and the regeneration of the skeleton. For instance, Figure 1 illustrates the musculoskeletal market.

The majority of the industry is focused on the large bones and joints. Remarkably, only in the United States, $30.6 billion is spent annually to treat bone related injuries. It can be predicted that this orthopedic sector will have a prevalent impact on the international healthcare business in the subsequent decade, spawning $100 billion in revenues globally with progress dependent on innovation (Girardi and Bros, 2007). Hence, significant research is being conducted on the need of biomaterials that would be appropriate for hard tissue replacement as well as reproduction. The potential to improve

the quality of health care using tissue engineering has driven many start-ups, pharmaceutical companies, and other firms to file several patents on new inventions (Pangarkar and Hutmacher, 2003). Integra Life Sciences, with revenues upwards of $101.2 million, deals with OnSatura ß-Tricalcium Phosphate® (TCP) as a synthetic bone void filler.

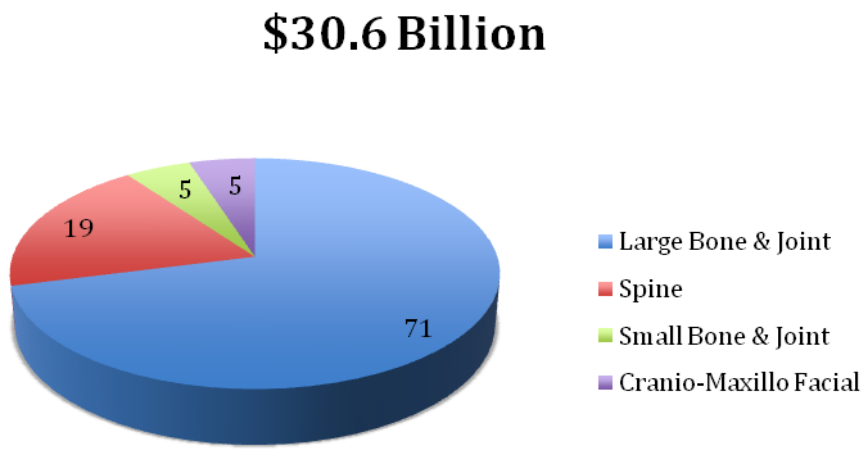

Figure 1. Muscoloskeletal Industry by sectors [adapted from Girardi and Bros (2007)]

Different studies show the use of ceramics, metals, and even alloys for replacement of bones. Moreover, surgeons have used autografts (tissue transplanted from one part of the body to another in the same person), allografts (tissue transplanted from one person to another of the same species), and bone grafts to recondition lost bone. It is projected that the regenerative medicine market encompassing stem cells, biomaterials, and tissue engineering will result in U.S. sales of more than $11 billion by 2020 (MaRS, 2009). During the 1990s, US Food and Drug Administration (FDA)/CE mark approved

biomaterials of natural and synthetic origin (Martina and Hutmacher, 2007). Thereafter, in the highly innovative world of tissue engineering and regenerative medicine, biodegradable polymers could be used as scaffolds to form a microenvironment for the cells.

Scaffolds should be able to mimic the host tissue and have biodegradable, osteoconductive, and biocompatible properties. It is important for the cells seeded in the scaffold to receive important nutrients, like oxygen, amino acids, and glucose, which enable them to proliferate. Figure 2 gives an insight into the engineered scaffold and how it can be used while incorporating growth factors as well.

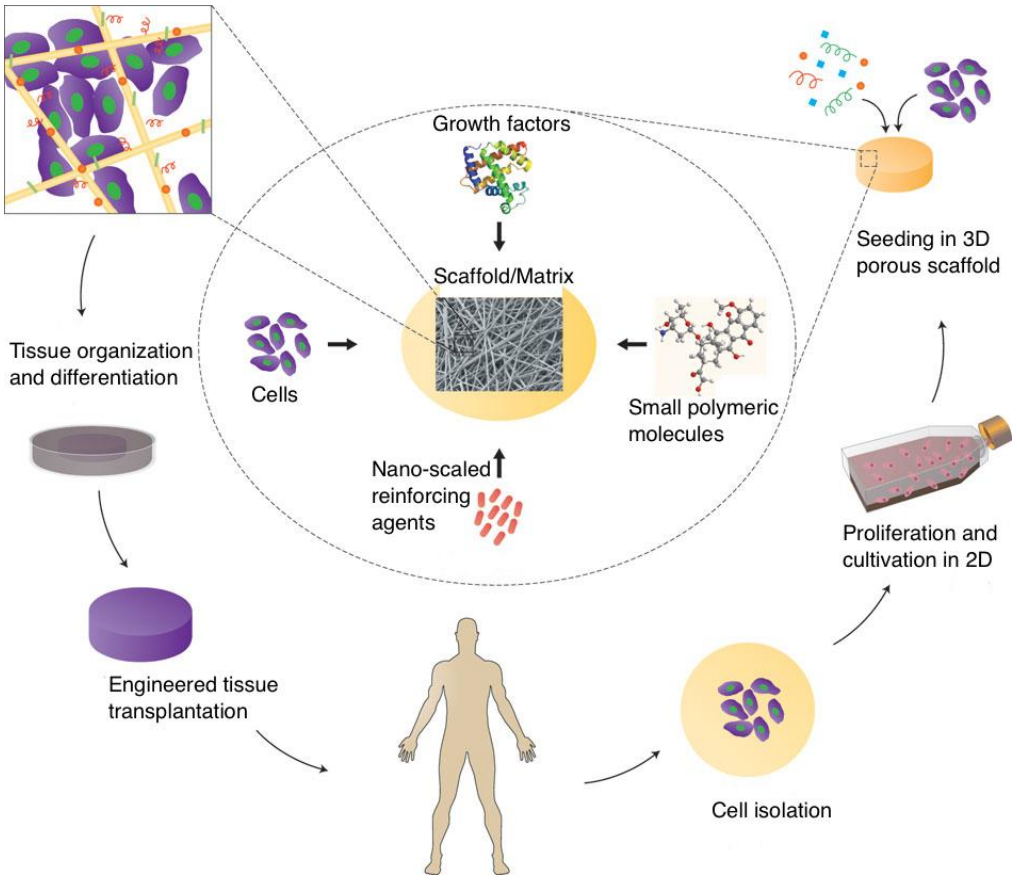

Figure 2. Tissue Engineering with scaffolds [adapted from Dvir et al. (2010)]

Materials like ceramics offer great bioactivity as scaffolds but due to their brittle nature fail to offer mechanical strength. Common polymers which have been investigated for bone repair applications include polyesters, polydioxanone, poly (propylene fumarate)(PPF), poly(ethylene glycol) (PEG), poly(orthoesters), and polyanhydrides (Porter et al., 2009). Polylactic acid (PLA) and its derivatives, pure PCL, polyglycolic acid (PGA) and its derivatives have been approved by regulatory agencies for use as scaffolds in bone and cartilage tissue engineering (Hutmacher, 2000; Gunatillake et al., 2003).

2.1.1 Mechanical Properties of Bone

Mechanical properties have been surmised in terms of compressive and tensile strengths. Compression strength determines the significant pressure at which materials that need to replace bone would get crushed. This shows the strength of a material that endures normal forces that act in the opposite direction of area vector. However, tensile strength helps in determining the force the material can undergo before it fails in mechanical integrity. One can determine how an object stretches and points at which it will show most and least flexibility until it reaches failure. The material endures axial forces that pull, like a string pulled along its free ends until it breaks. Every material has a certain threshold at which it fails.

Table 1 combines the significant figures that characterize human bone as well as soft tissue. The aforementioned scaffold needs to have features that match closely to the bones. The porosity of bone is usually between the range of 50-90% (Schmidt-Nielsen, 1984; Turner et al., 2001). Generally bone compressive strength goes up to 170 MPa and

tensile strength upwards of 200 MPa. However, in Table 1, it is observed that the iliac crest has one of the lowest tensile strengths of 0.12-8.2 MPa and compressive strength of about 3 MPa. Our focus lies on the versatile polyurethanes that possess the capability to be adjusted to the complex properties of this host tissue, as described below.

Table 1. Hard and soft tissue mechanical properties

Material	Compressive Strength (MPa)	Tensile Strength (MPa)	Reference
Bone	170	104-121	Schmidt-Nielsen (1984); Turner et al. (2001)
- Cancellous	4-12	2-5	Gibson (1985); Yang et al. (2001)
- Cortical	115-205	55-125	Hench and Wilson, (1993); Yang et al. (2001)
- Femur	180-209	104-120	Burstein et al. (1976); Goldstein (1987)
- Iliac Crest	2.75-3.26	0.12-8.2	Mosekilde and Mosekilde (1986); Goldstein (1987)
- Tibia	197-213	126-140	Burstein et al. (1976); Goldstein (1987)
Cartilage	25.8-35.7	9-40	Kerin et al. (1998); Holzapfel (2001)
Tendon	-	50-100	Holzapfel (2001)
Ligament	-	50-100	Holzapfel (2001)
Aorta	-	0.3-0.8	Holzapfel (2001)
Skin	-	1-20	Holzapfel (2001)

2.2 Polyurethane

These synthetic elastomers have extensively been used in various industries, like engineering, footwear, automotive, hoses & tubing, wiring & cables, construction and medicine, particularly as long-term medical implants such as cardiac pacemakers and vascular grafts (Gunatillake et al., 2003). The pliable mechanical properties and high biocompatibility have paved the way for the use of polyurethanes in regenerative medicine. One main characteristic of biodegradable polyurethanes and their degradation products is that they have shown minimum cytotoxicity in vitro and in vivo (Stankus et al., 2006; Tseng and Tang, 2007). The biodegradable polyurethanes are susceptible to hydrolysis and consequently degrade to form urea linkages and carbon dioxide gas, abundantly present in the human body. Blood regulates pH in the body between 7.35 and 7.45 by a number of homeostatic mechanisms to control the acid-base balance (Co and Dohme, 1899). When polyurethane degrades, there is a slight drop in pH due to the hydroxy acids, but high porosities (detailed in latter pages with scaffold properties) allow for better acid transport to the respiratory and urinary systems so that they can be dealt with by the pulmonary and renal regulations, respectively (Guan et al., 2005; Guelcher, 2008).

A significant aspect of polyurethane chemistry, visualized from Figure 3, is the presence of the urethane/carbamate bond (R_1NCOOR_2). This is formed when a diisocyanate reacts with a polyol with the help of a diol chain extender. The hard segment is composed of the polar mixture of diisocyanate and chain extender that are phase separated with the non-polar polyol in the soft segment. In Figure 4, it is observed that the hard domain is reinforcing the soft segment polyol. An interesting aspect is the

control of the diisocyanate/polyol ratios that are used to form the polyurethane molecule. The quantity of hard to soft segment used can manipulate the mechanical properties of the product. This is because under stress, the soft segment uncoils, leaving the hard segment aligned in the direction of the tensile stress. Studies like Huang et al. (1997) confirm similar findings where, regardless of the type of diisocyanate, the breaking stress increases with the hard segment content producing a detrimental effect on strain. The indicator of hydrogen bonds between the carbonyl groups in these diisocyanates is known as the Hydrogen Bonding Index (HBI), which holds the hard segments structrue. So, the ratio would affect the tensile and compressive strengths of the polymer, and also influence the melting temperature.

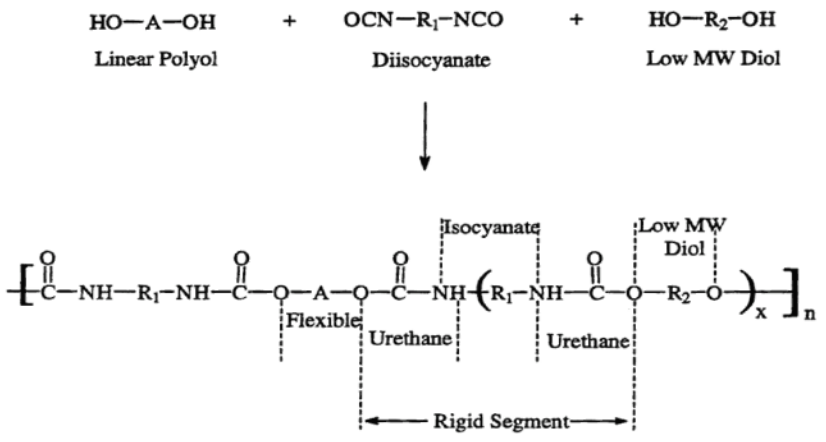

Figure 3. Polyurethane composition (Crawford and Teets, 1997)

The soft domain polyol is also known to have a hydrophobic nature whereas its counterpart in the diiscyanate is hydrophilic. Accordingly, the rate of in vitro biodegradation increases with content of polar hard domain and decreases with the soft segment content due to water repulsion and lack of hydrolysis (Skarja and Woodhouse,

1998). The control over degradation has a huge advantage in the field of scaffold engineering, as the rate the biomaterial degrades should closely simulate the rate at which the tissue regenerates. Compared to the degradation of polymers like PLA and PLGA, biodegradable polyurethane causes only a trivial change in pH. Moreover, the degradation products of polyurethane are shown to be non-toxic to endothelial cells, demonstrating linear degradation with lack of autocatalytic effects when evaluated against PLA (Martina and Hutmacher, 2007).

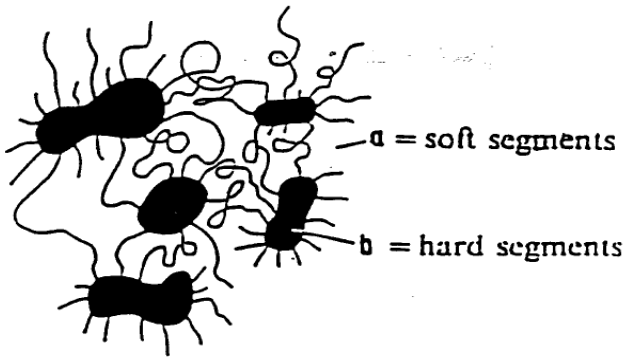

Figure 4. Domain morphology of polyurethanes (Crawford and Teets, 1997)

The type of polyol, diisocyante (aliphatic or aromatic), as well as the chain extender may also be varied to form different polyurethanes with different properties (Oertel and Abele, 1993). The aromatic methylene diphenyl diisocyanate (MDI) has been observed to degrade and release toxic phenyl groups in the body (De Groot et al., 1990; Lee and Tsai, 2000; Gretzer et al., 2003). 1,4-butane diisocyanate (BDI) has widely been used as a component of the hard segment to form biodegradable polyurethanes (Guan and Wagner, 2005; Heijkants et al., 2005a; Fujimoto et al., 2007; Guan et al., 2007). However, the use of BDI with putrescine (as chain extender) and PCL observed lack of cellular penetration (Siepe et al., 2006). Moreover, the compression modulus of 200 kPa

obtained was more applicable to fibrocartilage rather than large bones (De Groot et al., 1997a).

Separately, 2,6 diisocyanato methyl caproate (LDI, lysine-diisocyanate) has been used with PCL and butanediol (BDO) to synthesize polyurethane elastomers for soft tissue applications (Storey et al., 1993; Zhang et al., 2000; Asplund et al., 2007; Kızıltay et al., 2012). The polymers exhibited elongations at break exceeding 1000% and ultimate tensile strengths ranging from 7 to 34 MPa but with low-temperature properties that would be difficult to implement at 37 °C in the human body (Hassan et al., 2006). The hydrolysis of the ester group in lysine polyisocyanates yields a carboxylic acid group in the polymer, which has been conjectured to catalyze further degradation (Bruin et al., 1988).

For the soft segment, pre-polymers from poly(L-lactide-co-ε-caprolactone) diol and BDI have been composed to produce foam scaffolds with porosities of 75% and mechanical properties suitable for use as implants for knee-joint meniscus (Spaans et al., 2000). Adipic acid and water were used as chain extenders to produce carbon dioxide for porous structure, apart from the salt crystals; and surfactants with ultrasonic waves were used to regulate this pore structure. Structure-property assessments of degradable polyurethanes based on 2,6-diisocyanato methyl caproate, PCL, polyethylene oxide (PEO) and an amino acid chain extender show that PEO based polyetherurethanes were generally weaker than their PCL based counterparts (Skarja and Woodhouse, 2000).

Through meticulous research for the types of polyols used it was determined that PCL was the most widely used as segmented biodegradable polyurethane for regenerative

medicine with different isocyanates and chain extenders (De Groot et al., 1996, 1997b; Cohn and Hotovely Salomon, 2005; Chan-Chan et al., 2010). Furthermore, for the hard segment it was concluded that HDI, a linear diisocyanate, had degradation products that would not be harmful to the body (Gorna and Gogolewski, 2003; Matheson et al., 2004). This particular combination has been used in a previous study but with different chain extenders (Gorna and Gogolewski, 2002b; Grad et al., 2003; Tatai et al., 2007). Our novel blend with the copolymer chain extender using BDO, and the previously mentioned components, generates a new blueprint for segmented biodegradable polyurethane elastomers.

The mechanism for the synthesis of the polymer, and its resulting composition, is quite complex with different groups using different techniques. Usually, a two-step technique is used for the creation of the product, with the initial step producing a pre-polymer (or quasi-pre-polymer, in some cases) with different isocyanate to polyol ratios, and then that being incorporated into a chain extender for improved polymerization. MDI has been used with PCL to form pre-polymers with ratios 3:1, 2:1, 1.6:1 and 1.2:1 exhibiting a broad range of properties (Sánchez–Adsuar et al., 2000a, 2000b). Hence, similar ratios for pre-polymer composition were adopted for this study with higher PCL contents as well for the other end of the spectra. Figure 5 shows the polymer synthesis. The sequence and manner in which the monomers react, depends on the pre-polymer groups.

2.2.1 Synthesis and Characterization: A Closer Look

In a recent paper by Hood et al. (2010), HDI (as hard segment), BDO (as chain extender), and PolyEthylene Glycol (as soft segment) were used to synthesize segmented polyurethane. The product was filtered and rinsed with a 50:50 (v/v) mixture of ethanol and methanol and the precipitate was dried under vacuum at 50 °C for one week. They controlled the hard to soft segment ratios and found that the segments were confined using phase separation, which further helped selectively control crystallization. At a hard segment ratio of more than 50 wt%, morphological changes and mechanical properties could be manipulated (Hood et al., 2010).

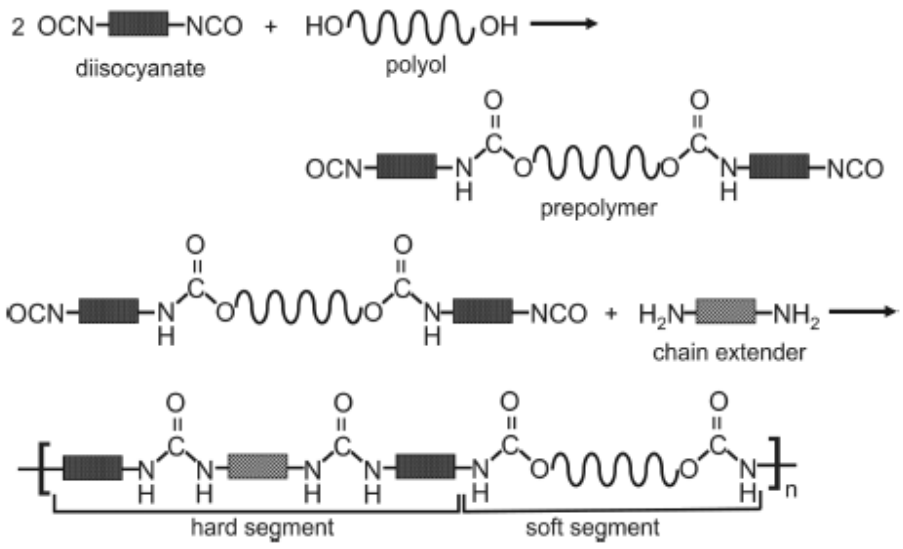

Figure 5. Polymer synthesis with pre-polymers and chain extenders for segmented polyurethane (Guelcher, 2008)

The storage modulus (stored energy in elastic portion) at 25 °C was found to be between 108-417 MPa using Dynamic Mechanical Analysis. Crystallization temperature and percentage of crystallinity reduced with increasing hard domain and amorphous PEG

at ambient temperature. Segments were incompatible with each other, causing phase separation in the nanoscale domains, helping to modify properties. Soft domains had lower melting temperature (T_m) than ambient temperature, compared to the melting temperatures of hard segment which they separate from.

Further characterization using Nuclear Magnetic Resonance (NMR) and Fourier Transform Infrared (FTIR) Spectroscopy confirmed the synthesis and composition of the polyurethane via the proton positioning and the functional groups for different corresponding peaks.

Studies showed that apart from hard domain content, mechanical properties are also dependent on the length of the polyurethane (Hutmacher, 2000). An increase in the molecular weight influences the chain length and therefore the strength (Fromstein and Woodhouse, 2002; Gorna and Gogolewski, 2006; Heijkants et al., 2008). As previously mentioned the hard to soft segment ratio (HDI:PCL) may be used to predict several behavioral trends in polyurethane. This is shown in an investigation by Sánchez-Adsuar et al. (1998) that demonstrates the effect of hard to soft segment ratio for different polyurethanes. The study shows that an increase in hard to soft segment (HDI:PCL) produces a greater difference between the weight average molecular weight (MW_w) and the number average molecular weight (MW_n) or simply an increase in polydispersity (Sánchez-Adsuar et al., 1998).

2.2.2 Non-porous Polyurethane Properties

Table 2 shows the tensile strength of different combinations of materials with different hard segment content. It is observed that varying polyols, isocyanates, and chain

extenders produces a large array of tensile strengths. Overall, the general trend observed in the literature was that the tensile and compressive strengths increases as the hard segment content is increased, but of course depending on the type of each amalgam.

Table 2. Mechanical properties of non-porous polyurethane with different hard segment content

Composition	Hard segment (%)	Tensile Strength (MPa)	Reference
Linear HTPBD, TDI, BDO	55	3.03	Brunette (1981)
Segmented HTPBD, TDI, BDO	55	18.6	Bengston (1985)
LDI, PEO, PCL	67	6-26	Fromstein (2002)
PCL, BDI, BDO	27	37.8	Heijkants (2005)
PCL, LDI	86.2	82.1	Guelcher (2007)

2.3 Scaffolds – Porous and Mechanical Properties

The properties of a scaffold require it to be structurally and mechanically similar to bone in order to function efficiently. Specifically, it is required that the pore size of the scaffold ranges from 150-350 μm and have porosity around 70%. In vivo, This is primarily so that the osteocytes (bone cells), which range from 10-30 μm (Leong et al., 2008), can properly embed into the scaffold. Moreover, it is critical for the structure to have interconnected pores that ensure the appropriate ingrowth of osseous tissue. In vivo, porosity also ensures that the phenomenon of vascularization, within the scaffold, takes place so that those nutrients that are vital for the proliferation of bone are present and

readily available. However, in vitro, low porosity kindles osteogenesis by sustaining cell proliferation and compelling cells to aggregate (Karageorgiou and Kaplan, 2005). Figure 6 illustrates the propagation of cells implanted in the polymer with significant porosity.

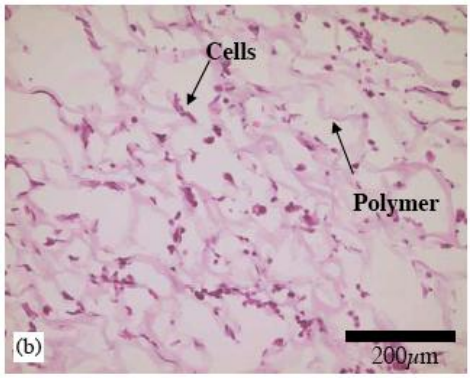

Figure 6. Polyurethane scaffold with osseous tissue growth (Guan et al., 2005)

2.3.1 Synthesis of Scaffolds – Procedures for Inducing Porosity

Porosity within the scaffold can be induced via various techniques, with certain advantages and setbacks, but the most important ones are salt leaching and phase separation. In the gas foaming method, the polymer is exposed to high pressure CO_2 and pores form as the gas evacuates the scaffold (Harris et al., 1998). It offers the advantage of no organic (toxic) solvents being used but handling at high temperatures and the lack of an interconnected structure has held back researchers from using this technique abundantly.

In the salt leaching method the scaffold is cast in a certain solvent and then added to crystals (usually NaCl) with the required size (Hou et al., 2003). The resulting material needs to be leached with a solvent (water if NaCl crystals are used) that can dissolve the crystals but not the polymer; subsequently, the initial solvent needs to be removed from the polymer via freeze-drying, or other evaporation (Heijkants et al., 2006). Concurrently,

the particulate step can be removed after the solvent dissolution by adding a diminutive amount of water instead, to form a blend. In a mold, the solution is then cooled down and freeze-dried to remove the liquid components, as before. This can be referred to as thermally induced phase separation (TIPS) method and has been used by quite a few papers in conjunction with the porogen leaching step (Tienen et al., 2003; Heijkants et al., 2004; Guan et al., 2005; Asefnejad et al., 2011). Figure 7 shows the structure of the scaffold with pores acquired using a combination of salt leaching and the TIPS methods.

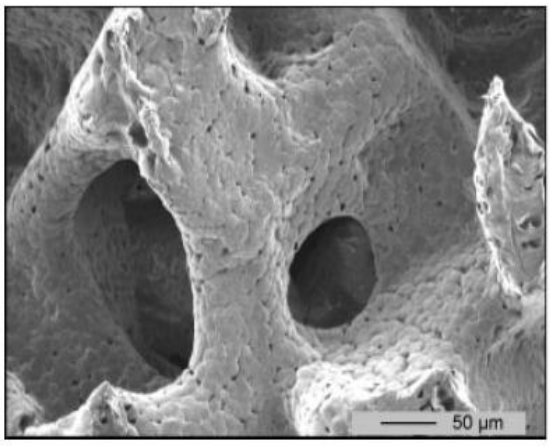

Figure 7. Porous polyurethane scaffold with interconnectivity (Heijkants et al., 2008)

2.3.2 Properties of Porous Biodegradable Polyurethane Scaffolds

Table 3 shows a comparison of materials of different porosities, resulting tensile strengths, compressive strengths and the amount of diisocyanate used. This table only engraves the fact that mechanical properties drastically diminish as the porosity is increased. It is known that inducing porosities of up to 75% in polymeric biomaterials can reduce mechanical properties of that material by more than 90% in most cases (Karageorgiou and Kaplan, 2005). The study using Estane produced a compression

moduli of 40 kPa for a porosity of 87% and up to 400 kPa for a porosity of 73% (Heijkants et al., 2006). Figure 8 shows this phenomenon. These porous scaffolds showed improved interconnectivity, compared to previous studies, and are claimed to have better applications for meniscus lesions. Similarly, the scaffold obtained in the Gorna study have potential to be used as cancellous bone graft substitutes and in the repair of articular cartilage (Gorna and Gogolewski, 2006)

Table 3. Mechanical properties of porous scaffolds with different HS content and porosity

Composition	Hard segment (%)	Porosity (%)	Compressive Strength (MPa)	Tensile Strength (MPa)
PCL-b-PEG-b-PCL and BDI and putrescine (*)	33	91.5	-	1.68
PCL and BDI and putrescine (*)	33	93.7	-	0.97
PCL BDI and BDO (HS) (**)	12	81	1	-
PCL, diisocyanate, isosorbide diol (***)	60	75	0.8	-

* Guan (2005), ** Groot (2008), *** (Gorna 2006)

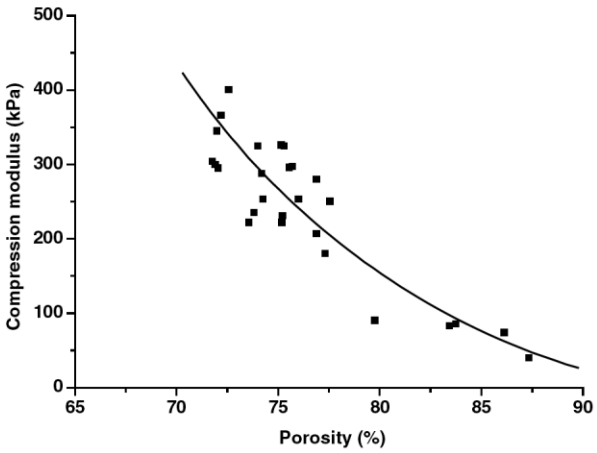

Figure 8. Influence of porosity on compression in scaffolds (Heijkants et al., 2006)

2.4 Reinforcement of Polyurethane

The primary goal of this exercise is to strengthen the scaffolds once their mechanical properties have been reduced due to the porosity. In this review, we specifically focus on the use of nano-particles for reinforcement of polyurethane. Hydroxyapatite (HAp) is a bioceramic that makes up about 60% of the bone. Studies show nano-HAp as inorganic fillers in polymers not only increase the mechanical properties of the construct, but also enhance its bioactivity and osteoblast adhesion (Gorna and Gogolewski, 2002a). Also, the acidic resorption products of the aliphatic polymer would be buffered by the basic resorption by-products of HAp and may thereby assist to prevent the development of an adverse atmosphere for the cells due to declined pH (Shikinami et al., 2005).

For incorporation, initially, the reinforcement requires that the nano-scaled reinforcing agent be dissolved or suspended in a common solvent. For instance, carbon nanotubes (CNT) were dissolved in dioxane, the Bioglass in 1-methyl-2-pyrroloidone and

the cellulose nanocrystals (CNC) were sonicated in DMF (Marcovich et al., 2006; Jell et al., 2008; Ryszkowska et al., 2010).

Many researchers have reported different mechanisms to incorporate the solution containing the reinforcing agent during polymerization. For instance Jell et al. (2008) dissolved Estane (a readily available industrial polyurethane) in the dioxane/CNT mixture with a 5 wt% content of the former. This was then sonicated and frozen at -25 °C after which it was freeze-dried to remove the dioxane. Ryszowska et al. (2010) mixed the Bioglass in the solvent with PCL, and this filler was added to the polyurethane. Marcovich et al. (2006) incorporated the polyol into the CNC solution. Consequently, before this was integrated with the pre-polymer, the DMF was evaporated. Another study that dealt with the drug loaded ethyl cellulose microspheres added 50 or 100 mg of these per scaffold after polymerization had taken place at about 65 °C (Liu et al., 2010).

2.4.1 Mechanical Properties of Nanoreinforced Polyurethane

Figure 9 is an illustrative representation of the reinforcement on a nano-scale. A similar force is applied to both non-reinforced and reinforced polyurethane with hard and soft domains. The non-reinforced model observes stretching and distortion of the polyurethane matrix. However, those that are reinforced are better able to hold the structure and hence observe greater mechanical properties. Further, the degree of attraction of the reinforcing agent to the hard domain is more clearly understood.

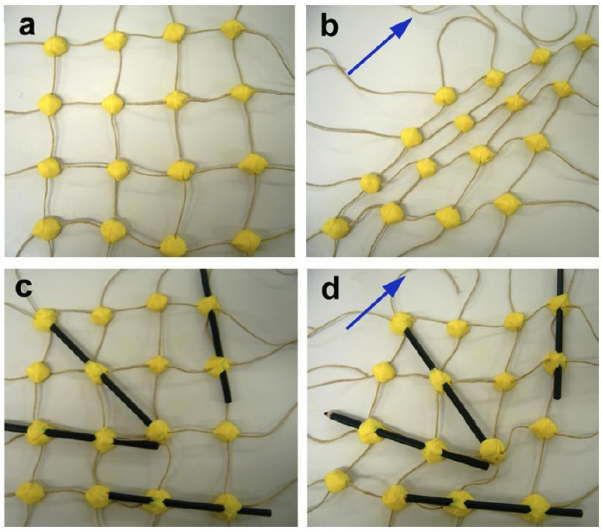

Figure 9. Model for polyurethane network (a) with yellow blocks representing hard domains and brown ropes as soft segments (b) stretching in the direction of the blue arrow (c) reinforced with nanotubes in hard segment (d) stretching with reinforcement improving strength (Fernández-d'Arlas et al., 2011)

Table 4 shows the compressive strengths of different scaffolds with varying content and type of reinforcement. This is a basic pictorial representation of the percentage increase in strength achieved in various studies, and whether they had porosity induced. It can be seen that Estane with a 5 wt% of CNT showed an increase in compressive strength of 200% but did not have any porosity and had minimal strength (Jell et al., 2008). Comparatively, 70% porosity was achieved in scaffolds reinforced with almost 20 wt% Bioglass to increase the strength by 340% (Ryszkowska et al., 2010). The bioactivity of these scaffolds was confirmed by the layer of hydroxyapatite formed on the surface of the foam when kept in simulated body fluid (SBF). Although, these mechanical properties are enhanced using nano-reinforcement, they can hardly match the high compressive strengths of bone, except for those of the iliac crest.

Table 4. Mechanical properties of reinforced polyurethane scaffolds with different reinforcing agents and contents

Composition	HS (%)	Porosity (%)	Type of Reinforcement	Wt (%)	Change in Compressive Strength (%)	Reference
Diol, MDI	32.1	0	Cellulose Nanocrystals	5	143*	Marcovich (2006)
HDI Cross-linked aerogels	6, 20, 34	62-96	Carbon Nanofibers	2,5	~300	Meador (2008)
PEG, HMDI, BDO w/ HA	46	83	Drug loaded Ethyl Cellulose microspheres	19.6	13.14	Liu (2010)
HMDI, PCL, PEG	22	70	Bioglass	5-20	340	Ryszkowska (2010)

* Instead of compressive strength, reported tensile modulus (no tissue regeneration applications, hence no porosity either)

2.4.2 Reinforcing Agents

Jell et al. (2008) have enhanced polyurethane scaffolds using carbon nanotubes, as shown in section 2.4.1. SEM was utilized to determine the pore size of the scaffolds, which was in a range of 30-124 µm. Porosity and foam density were used to calculate the specific pore volume at about 10 cm^3/g, and both these characteristics are seen to be sufficient for vascularization. The compressive modulus was enhanced with the increased addition of CNT in the polyurethane matrix. The mechanical property was tested using the universal testing machine with a 1 kN load cell moving at 20 mm/min at a strain of 75%. The study also included further cell analysis claiming that proliferation of

osteoblasts was evident, however, the CNT additionally manipulated cell behavior and might cause unwanted phenotypic characteristics (Jell et al., 2008).

Carbon nanotubes and nanofibers produce sufficient increase in strength with respect to the porous biomaterials, but their detrimental ability to modify cell phenotype makes them less biocompatible. Hence, the search for superior reinforcing agents, like biocellulose nanofibers, is warranted. Their biocompatible properties were highlighted in a study on rats, showing no signs of inflammation, and a lack of abnormally high number of cells and foreign body reactions around the biocellulose implant, confirming integration with the connective tissue (Helenius et al., 2006). The lack of biodegradability was corroborated with another rat study that showed a reduction of about half the size of the implant in a period of 60 weeks, suggesting a probable reduction of biodegradability in a biocellulose fiber reinforced scaffold (Märtson et al., 1999).

A study using commercial grade starch with biocellulose as a composite shows that the tensile strength increased from 31.06 MPa to 131.1 MPa, with a 400% change with 22% concentration of cellulose (Wan et al., 2009). Biocellulose nanofiber composites have found many applications in the biomedical field and research has been conducted in the areas of sensors, drug delivery vehicles, scaffolds and valves (Hubbe et al., 2008). Examinations on microporous biocellulose implants for bone scaffolds found a low Young's modulus of 1.68 MPa, a tensile strength of 0.22 MPa, and a strain at break at 26.9%, but sufficient adhesion of cells in 2/3 of the 100 µm pores (Zaborowska et al., 2010). It can be suggested that the depleted mechanical properties of the implant due to water uptake will be removed if they were used for reinforcement of polyurethane biocomposites

For further details on the benefits and superior properties of this innovative product, readers are redirected to various reviews and studies conducted by our research group (Dahman, 2009; Sani and Dahman, 2009; Dahman and Sani, 2010; Dahman et al., 2010; Khan and Dahman, 2012).

In summary, it was evident from the review of articles that reinforcements, specifically in the nano-scale, hold lots of potential to enhance the performance of the polyurethane scaffolds. This phenomenon, in combination with an assortment of biodegradable compositions of different diisocyanates and polyols in manipulated ratios gives rise to porous scaffolds with enhanced, flexible physical properties. The applications in this aspect range from use in weaker bones to other soft tissue but emphasize the fact that the search for the perfect scaffold for bone tissue engineering is far from over. Against this background we postulated that it would be essential to examine the novel green nanofibers as reinforcing agent into the continuous matrix of polyurethane with an innovative composition using linear HDI. This is a pioneer investigation and hence no comparative data is available for polyurethane scaffolds with nanofiber reinforcement. Thus merits the following study on green biomaterials, which shows illustrious possibilities in the versatile world of tissue engineering.

CHAPTER 3

MATERIALS AND METHODS

3.1 Materials

All chemicals were purchased from Sigma-Aldrich and were used as received unless stated otherwise. Polycaprolactone diol [PCL; M_n=2000 g/mol; Figure 10(c)] was used as the soft segment (SS) in polyurethane matrix and was dried under vacuum for 2 days prior to use. Hexamethylene diisocyanate [HDI; M_n=168.2 g/mol; Figure 10(b)] was used as the hard segment (HS) and was distilled under vacuum pressure prior to use. 1,4-Butanediol [BDO; M_n=90.1 g/mol; Figure 10(a)] was used to synthesize the copolymer chain extender.

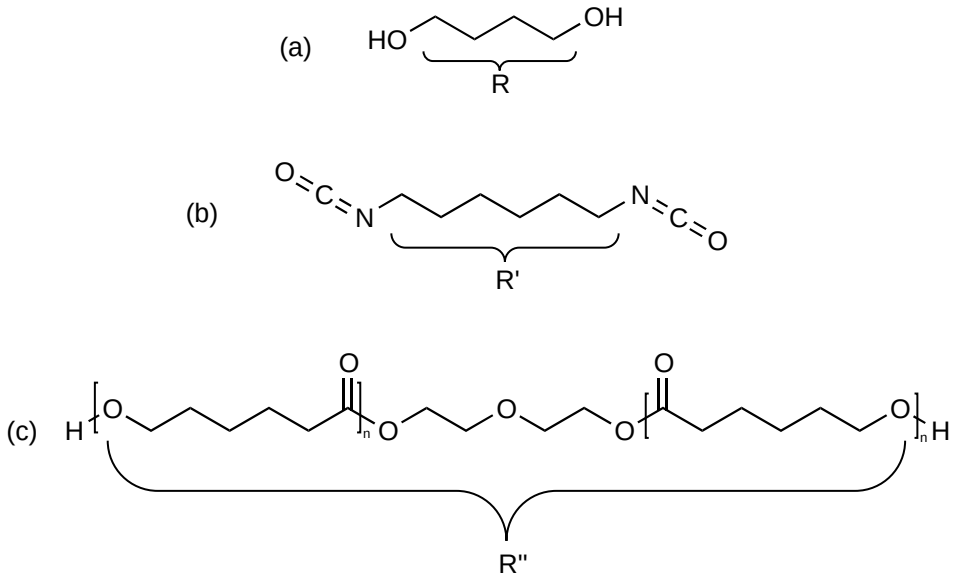

Figure 10. Molecular structure of (a) 1,4-butanediol (BDO) (b) Hexamethylene Diisocyanate (HDI) and (c) Polycaprolactone Diol (PCL)

Dimethyl sulfoxide of ACS reagent (DMSO; M_n=78.13 g/mol; purity 99.9%+) was used in the present work as the common solvent for polyurethane. The deuterated version of the solvent (DMSO-d_6; 99.5+ atom % D) was used for NMR analysis. Sodium Chloride (NaCl) salt (SigmaUltra (99.5%); +80 mesh (≥98%); M_n=58.44 g/mol) with well-defined particle crystal sizes was used for the creation of porous structure in scaffolds. Biocellulose nanofibers were synthesized as described below, and were provided in the form of suspension solution with the concentration of 42 g/L.

3.2 Experimental Setup for Polymerization Reaction

As seen in Figure 11 below, polymerization reactions were conducted in a 1000 mL reaction vessel with a five neck head sealed with a flange (Ace Glass; Vineland, NJ). This was equipped with an overhead stirring shaft driven by a motor (Heidolph RZR 2020; Schwabach, Germany), a reflux condenser, and a nitrogen gas inlet that were contained in three of the necks, while the other two were used for chemical feed and sampling. Polymerization reactions were conducted in DMSO solvent at 80 °C. This was the temperature of the oil bath in which the reactor was immersed. The polymerization reaction temperature throughout this study was controlled using an electronic contact thermometer with a fuzzy logic controller (VT-4; VWR) and a magnetic hotplate stirrer (VMS-C7; IKA, North Carolina). All polymerization reactions were performed under nitrogen blanket to control oxygen content and minimize all unwanted reactions. All reaction components were mixed at a fixed stirring speed of 800 rpm through a pitched blade impeller fixed to a shaft (Heidolph PR 30 and 39; Schwabach, Germany). These had a propeller diameter of 58 mm and 75 mm, respectively, and were driven by the

Heidolph RZR 2020 motor. The glass reflux condenser was cooled by tap water to condense back polymerization solvents.

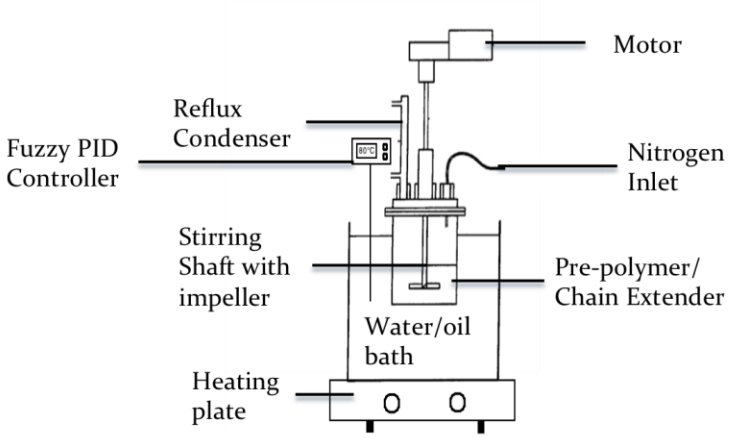

Figure 11. Glass reactor assembly for polyurethane synthesis with mechanical stirring at 80 °C

At the end of each polymerization reaction, polyurethane polymers were dried and purified from the DMSO solvent by heating at 50 °C under vacuum using a Rotary Evaporator (RotaVap; Labconco, Kansas City, MO). This RotaVap was operated at 40 rpm under vacuum pump, while the polymer solution was immersed in a water bath at 50 °C to evaporate DMSO (boiling point of 189 °C).

In the present study, 21 total different samples were synthesized. They can be classified under the following groups:

- Group I that contains five samples of basic polyurethane continuous matrices with different compositions of hard to soft segment molar ratios (4:1, 2:1, 1:1, 1:2, and 1:4).
- Group II that contains five porous samples of basic polyurethane in Group I

- Group III contains five samples of polyurethane biocomposites, which consist of the porous polyurethane matrices (from Group II) reinforced with 5 wt% of biocellulose nanofibers (BCNF) with respect to polyurethane
- Group IV contains six samples of the polyurethane biocomposites as in Group III. These six samples are mainly synthesized from the three porous sample of polyurethane from Group II (2:1, 1:1, and 1:2 HDI:PCL molar ratios) with reinforced biocellulose nanofibers at two higher concentrations of 10 and 15 wt% with respect to polyurethane.

3.3 Syntheses of Polyurethane Polymers

Polyurethane matrices of different compositions were synthesized in the present work in three main steps as follows:

3.3.1 Synthesis of Chain Extender

The chain extender copolymer (BDO/HDI/BDO) was prepared by mixing hexamethylene diisocyanate (HDI) with six-fold excess of 1,4-Butanediol at 80 °C. The mixture was heated at 80 °C for four hours under nitrogen atmosphere. At the end, excess BDO was removed by washing with distilled de-ionized (DDI) water followed by dry acetone. The finished product was in the form of a white semi-solid substance.

3.3.2 Synthesis of Pre-polymer

In order to synthesize polyurethane with different ratios of hard to soft segment, the pre-polymers were prepared by reacting PCL with variety of ratios of HDI at 80 °C

for 4 hours under nitrogen atmosphere using the same experimental setup in Figure 11 above. The molar stoichiometric ratios of HDI:PCL were 1:4, 1:2, 1:1, 2:1, and 4:1 molar. Excess HDI (boiling point of 255 °C) was removed by evaporating at 70 °C under vacuum using the RotaVap.

3.3.3 Synthesis of Polymers

The chain extender copolymer (BDO/HDI/BDO) was initially dissolved in DMSO at concentration of 50 wt% at 80 °C. Equal weight of the pre-polymer was then added to the mixture [weight ratio of 1:1 for (BDO/HDI/BDO):(HDI/PCL)]. The reaction time was 30 minutes under nitrogen atmosphere, using the same experimental setup as in Figure 11 above. The resulting polymer was precipitated in water. To remove the excess solvent, the product was washed initially with 20% ethyl alcohol in water and finally with 96% ethyl alcohol in water. The finished product was dried under vacuum at 45 °C for 1 week in a vacuum oven.

3.3.4 Biocellulose Nanofibers Synthesis

Green biocellulose was produced via Simultaneous Saccharification and Fermentation (SSF) depending solely on the renewable resources of agricultural residues (Al-Abdallah, 2012). Wheat straw was used as the fermentation carbon source; it was pretreated with 1% dilute sulfuric acid, and then adjusted to the proper fermentation conditions by Acetobacter Xylinus bacterium. The course of biocellulose fermentation production lasted for 7 days, and then the solution was treated with excess NaOH at 100 °C for cell lysis. 5 runs of repeated washing and centrifugation extracted the

produced biocellulose. Stock solution of these novel biological nanofibers was stored as suspension solution with the concentration of 42 g/L.

3.4 Preparation of Porous Structure of Polyurethane Samples

To develop the porous structure of polyurethane, NaCl of known crystal size range was used in the present study. Specific crystal sizes of NaCl were obtained using Retsch mesh standard testing sieves (Haan, Germany) between the range of 125 and 355 μm (DIN 4188 and ISO 3310). In order to isolate the required particle size, the salt was initially dried overnight in an oven at 115 °C. The salt particles were then poured on to the 355 μm sieve and collected over the 125 μm sieve. The sieves were mounted on a MaxQ automated shaker (SHKA4450; Thermo Scientific, Dubuque, Iowa) to speed up sieving the salt particles.

After obtaining the required crystal size of the salt, polyurethane samples were heated at 80 °C and dissolved in DMSO at 20 wt% in order to lower the viscosity. This allowed for better mixing of the NaCl crystals with the polymer matrix that were added at ratios of 2.5 g of salt per gram of polymer. DDI water was then added to the solution at 5 wt% relative to DMSO to decrease the concentration of the solvent, as explained in section 4.3. Final mixture was stirred using a magnetic stirrer for about 30 minutes at 80 °C ensuring achievement of homogenous mixtures.

After mixing, the resulting mixture was poured into the predesigned and fabricated mold (ASTM E8; Appendix B) to produce the prototype with the required dimensions. The mold was then placed in an ultra low freezer (Revco Elite Plus; Thermo Scientific, Asheville, NC) for rapid cooling at -80 °C for about 30 minutes. Then the

polymer sample was ejected from the mold. Subsequently, it was introduced to a bath of 20% ethanol in water solution and the NaCl and solvent were washed out through leaching. This was done by pressing under ethanol in DDI water at room temperature for a day. The bath was gently changed twice during this leaching process. Immediately thereafter, samples were dried under vacuum in order to circumvent degradation and maintain the porous structure of the final prototype (Hou et al., 2003; Heijkants et al., 2004; Guan et al., 2005).

3.5 Reinforcing of Biocellulose Nanofibers in Polyurethane Matrices

Biocellulose nanofibers were obtained in DDI water as suspension with initial concentration of 42 g/L. The nanofibers were transferred into DMSO by stepwise solvent exchange and were left to get swollen for 72 h. Transfer procedure was done using barrel-shaped filter funnels with fritted glass disc of 0.45 micron opening, which was connected to a conical flask that works under vacuum. Nanofiber suspension solutions were placed in the funnel and the water was filtered out under vacuum with continuous mixing, while DMSO was added to the funnel simultaneously. This solvent exchange method was pursued to ensure almost complete removal of DDI water.

Biocellulose nanofibers were used in the present study as the reinforcement agent, which were added to the different polyurethane samples during the porous structure development described in section 3.4 above. In detail, 20 wt% polyurethane samples were initially dissolved in DMSO at 80 °C, and 2.5 g of NaCl crystals of the required size were added. At the same time, 5 wt% water was added as the non-solvent. Consequently, DMSO was included that contained the required biocellulose nanofibers contents. The

mixture was mixed under continuous stirring to ensure homogeneity. Three main levels considered for nanofiber content were examined: 5, 10, and 15 wt% with respect to polymer weight.

Thereafter, the mixture was poured in the appropriate mold and was placed in the ultra-low freezer at -80 °C for 1 hour. The removed scaffold was then transferred to 20% ethanol bath to remove and wash out the solvent and the NaCl crystals by leaching (washing with water) and then dried under vacuum to maintain the final porous structure (Jell et al., 2008). Two types of molds were utilized in the present study to prepare final samples for the mechanical testing (compression and tensile analysis). More details on this are presented in the following section.

3.6 Analytical Techniques to Characterize the Final Composite Samples

3.6.1 Fourier-Transformed Infrared (FTIR) Spectroscopy

Fourier-transformed infrared (FTIR) spectroscopy was used in this study to characterize the functionality of the different polyurethane compositions. This analysis gives spectral information, which presents a molecular layout of the material. It is possible to obtain data on the functional groups of the material as dispersions in non-absorbing (inert) matrices of potassium bromide (KBr). The sample is exposed to infrared radiation which, depending on the functional groups, is absorbed or transmitted through at different wavelengths. This is how specific functional groups can be appointed in the spectral range, and these are neither influenced by temperature nor pressure.

Perkin Elmer's FTIR Spectrometer 100 series, Model Spectrum 1, V3.01 (Waltham, USA) equipped with the Spectrum 6 software was used to characterize the different segmented polyurethanes. A 68340 integrated chip was used to process signals with a mid-range deuterated triglycine sulfate (FR-DTGS) infrared detector. 32 scans were accumulated in the range of 4000 to 400 cm^{-1} at a resolution of 2 cm^{-1}. Infrared spectra of the polymers were recorded in % Transmittance mode.

For the sample preparation, about 5 mg of shredded samples were dried under vacuum and then grinded with 500 mg of KBr. The samples were ground and mixed using a mortar and pestle, and pressed to create pellets that were used to generate the spectra. Background on pure KBr pellet was initially run, for conditioning, and then the sample, as is common practice before acquiring data. FTIR patterns of polyurethanes containing different ratios of pre-polymer HDI:PCL (hard to soft segment) were compared to observe any differences among them (as well as to confirm starting materials).

Table 5 shows common FTIR characteristic wavelength bands obtained from an assortment of comparative references (Heijkants et al., 2008; Hood et al., 2010; Asefnejad et al., 2011).

Table 5. Polyurethane band assignments in FTIR

Wavelength (cm^{-1})	Band Assignment
3320	NH stretching
2935	$-CH_2$ stretching, asymmetric
2868	$-CH_2$ stretching, symmetric
1729	Non-hydrogen bonded C=O
1682	Amide (H-bonded) (RCONHR')
1542	NH vibrations
1294-1464	$-CH_2$ vibrations

3.6.2 ^{1}H Nuclear Magnetic Resonance (NMR) Spectroscopy

NMR spectra of the samples were recorded using a Bruker 400 MHz Spectrometer by Bruker Biospin (Rheinstetten, Germany) in deuterated DMSO (DMSO-d_6; 99.5%) solvent to quantitatively characterize the composition of polyurethane matrices. All NMR routine experiments done by this spectrometer are run via automation at room temperature (i.e. 25 °C).

^{1}H NMR is an important tool for elucidating structural composition in organic chemistry. Atoms that have an odd number of protons (or neutrons), like ^{1}H, can be studied using this method. The magnetic spin in the nuclei cause them to orient in a particular direction when a magnetic field is introduced. The energy state is influenced by the field strength (or frequency) and can permit analysis of up to 5% accuracy. Electrons that surround the nucleus produce dissimilarity in the resonant frequencies (compared to reference frequencies) known as chemical shifts (δ). The NMR spectrometer is composed of magnets, a radio frequency transmitter and receiver (generating magnetic fields), a

sweep generator (delivering and detecting fields to and from the sample), a sample tube holder, and a computerized recorder for spectrum processing and acquisition.

In this study, 5 mg of the novel material was dissolved in approximately 0.5 mL of DMSO-d_6. At larger quantities of polyurethane relative to DMSO, the solubility was naturally reduced, but NMR peaks were less prominent which brings in the need to establish an appropriate sample quantity. Magnetic stirring, heating, ultra-sonication (Bransonic ultrasonic cleaner model 3510R-DTH by Branson Ultrasonics Corp., Danbury, CT) shaking, and filtering ensured pure and completely soluble mixtures. This was placed in 5 mm O.D. tubes (Wilmad-LabGlass) and chemical shifts were recorded. The minimum height of the tubes with which the NMR analysis would be operable was 5 cm and the sample solution needed to be at that level. The sample was loaded inside a strong magnetic field where the effects of the field in the nucleolus of every hydrogen atom in the molecule were detected, and thus, permitted the analysis of the structures. NMR tubes were washed with ethanol about 5 times to avoid contamination.

3.6.3 Scanning Electron Microscopy (SEM)

Morphological study of the final polyurethane based scaffold was conducted using a scanning electron microscope (SEM) with high-resolution images. SEM is a type of microscope that produces an electronically magnified image of a specimen for detailed observation. The electron microscope uses a particle beam of electrons to illuminate the specimen and electromagnetic "lenses" are used to control this electron beam and focus it to form a magnified image. In order for proper depth and surface morphology to be viewed in the structure, images need to be viewed with the electron microscope that gives

off these beams. Electron microscopes are used to observe a wide range of biological and inorganic specimens including microorganisms, cells, large molecules, biopsy samples, metals, and crystals.

Pore size, distribution and interconnectivity was addressed using images developed by SEM. Cross-sectional samples were vacuum dried on aluminum SEM holders and sputter coated with a 10 nm gold layer. Mr. Li handled the mounting and obtaining of SEM images from this point. The JEOL/OE equipment model JSM-6380 LV (Oxford Instrument, U.K. - software version SEI England) with a monochromator (Al X-ray source) was operated between 5-20 kV generating high-resolution images. The samples were then analyzed between a magnification of x30 and x100 for porous structure and x20k for biocellulose nanofiber reinforcement. The pore sizes were measured using the software provided by the instrument or manually using the scale bar given by the SEM image.

3.6.4 Porosity Estimation

Porosity was estimated using the straightforward technique of ethanol displacement (Guan et al., 2005) according to Equation I. Ethanol was used as the displacement fluid as it effortlessly breached into the pores and did not provoke reduction or enlargement of the polymer, unlike water. A known volume of ethanol (V_1) was contained in a graduated cylinder and a portion of the dry scaffold was immersed in. The container was kept under vacuum until air bubbles were able to expel from the scaffold and consequently the liquid displaced and permeated the pores. The final volume (V_2) of the ethanol with the ethanol-impregnated scaffold was measured. Later the scaffold with

liquid was removed and the remaining volume (V_3) was recorded. Porosity was calculated as follows:

$$P = \frac{(V_1 - V_3)}{(V_2 - V_3)} \times 100\% \quad (1)$$

where $(V_1 - V_3)$ is the amount of liquid taken up by the scaffold and $(V_2 - V_3)$ is the volume of the scaffold with ethanol.

3.6.5 Mechanical Properties of Polyurethane Polymers and their Composites

Mechanical tests were performed on all samples to quantify compressive and tensile strengths. The yield tensile and peak compressive forces of the 3-D samples were measured using a Universal Testing Machine (Smart Table Model (STM) – 50 kN; United Testing, Concord, ON), as shown in Figure 12. This was equipped with a 500 N load cell operating at a crosshead speed of 10 mm/min (for tensile) and 2 mm/min (for compressive). The strengths were calculated as follows:

$$P = F/A \quad (2)$$

Where,

F is the breaking force in Newtons, A is the cross-sectional surface area in mm^2, and P is the pressure in MPascals.

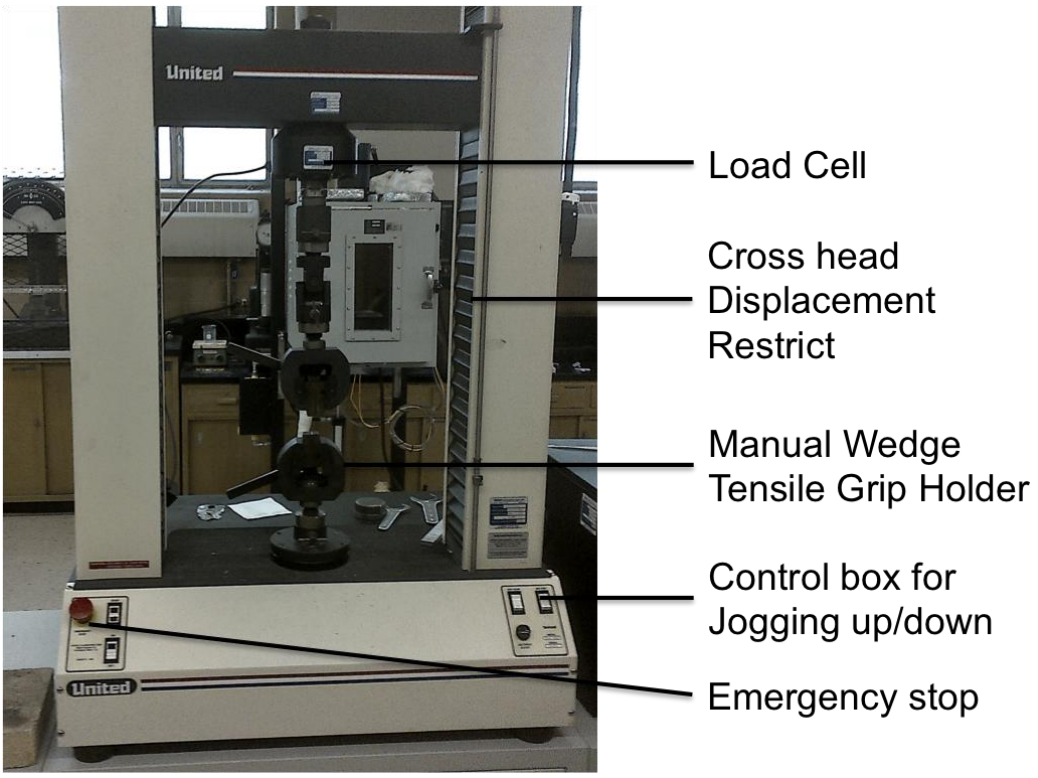

Figure 12. Universal Testing Machine (UTM) for mechanical testing in tensile mode

Figure 13 shows the tensile standard with a 6 mm thickness, 6 mm width and 100 mm length with a dumbbell shape. Both molds had the same cross-sectional area of 36 mm^2 (6 mm x 6 mm; ASTM E8; Appendix B). Further details about the ASTM E8 standard test methods for mechanical tension testing of materials are presented in Appendix B. In Equation II, the force at which the samples disintegrated was determined by the highest peak and this was divided by the area. DATUM software was used to analyze the measurements from the machine. All the given values were a result of three or more measurements. For tensile analysis the grip portion of the sample was clamped and for compressive analysis the prototypes were placed between two plates.

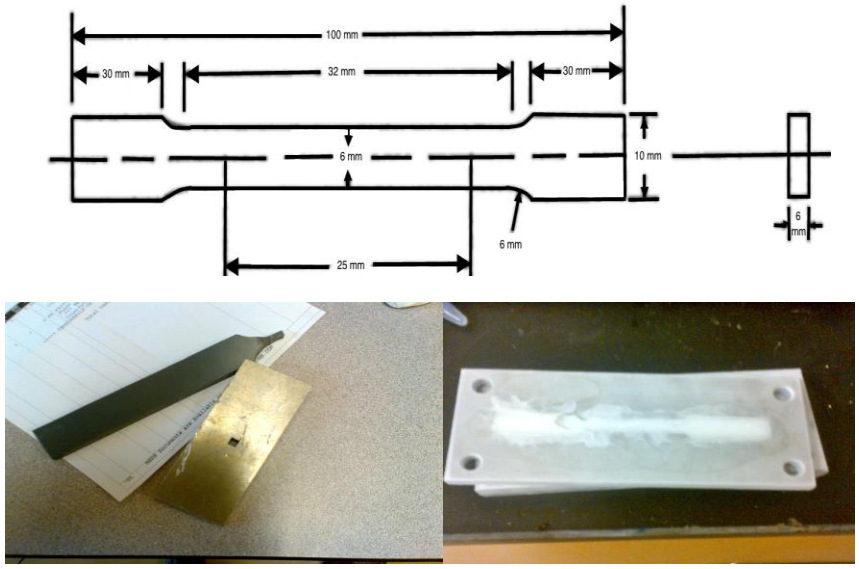

Figure 13. ASTM E8 standard size (Appendix B) with dimensions, and mold for compressive samples (left) and tensile samples (right)

Figure 14 shows the samples that were ejected from a mold and adhered to the standard dimensions. The figure also shows the mold for the compressive samples which was designed to be a cubic 6 mm x 6 mm x 6 mm. Plastic tools (anti-molds) for removal were necessary so that breakage could be avoided by even application of pressure for ejection.

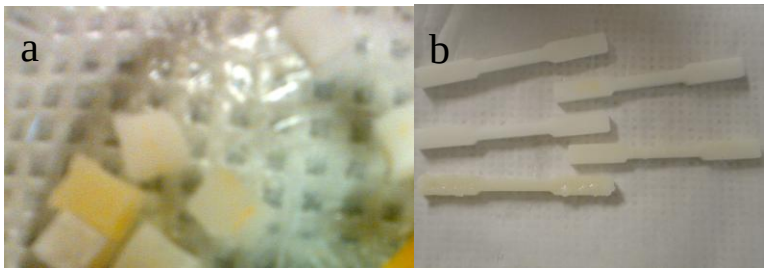

Figure 14. Various samples for (a) compressive and (b) tensile testing

The molds for the polyurethane samples were manufactured according to the dimensions set by the American Society for Testing and Materials (ASTM) E8 (E28 Committee, 2011) and listed in Figure 36 in Appendix B.

3.7 Reproducibility of Results and Error Analysis

Each composition that was proposed in the present work was produced and mechanically tested at least three times, and the reported results represent the average value of the data amassed. Table 9 (see Appendix C: Raw Experimental Data) shows results that were measured for the reproduced samples of compressive strength in non-porous, porous, and reinforced scenarios. Error percentages were calculated for all results reported based on the replicated mechanical test of the scaffold samples and were in the range of: 0.1 to 11.7 % for basic polyurethane matrices; 6.6 to 10.3 % for porous polyurethane samples and 7.7 to 12.6 % for biocomposite samples. It is noteworthy to mention that experimental errors were offset by a few outlying blends and do not reflect negatively on the overall reproducibility of this study.

It is also important to note that the values for strength have a larger range for the nanofiber containing scaffolds compared to the non-reinforced samples. This variability can be ascribed to the fact that even minute agglomerated nanofibers can cause micro- or nanoscopic faults within the samples (Buffa et al., 2007).

The standard deviation (σ; Equation III) was calculated according to the following simple equation.

$$\sigma = \sqrt{\frac{\sum(x-\bar{x})^2}{(n-1)}} \qquad (3)$$

Where,

$\bar{x}$ = sample mean value; n = sample size;

The Relative Standard Deviation (%RSD; Equation IV) was calculated from the value of STDEV. The %RSD can be written as:

$$\%\ RSD = \frac{\sigma}{\bar{x}} \times 100\% \quad (4)$$

Where,

STDEV = standard deviation of the samples;

CHAPTER 4

RESULTS AND DISCUSSION

4.1 Chemical Pathway of the Polyurethane Synthesis

Final biodegradable porous polyurethane for reinforcement with biocellulose nanofibers were synthesized through three synthesis steps as follows:

First step comprised the formation of the copolymer chain extender (BDO/HDI/BDO). In this step, the low molecular weight 1,4-butanediol [BDO; Figure 10(a)] reacts with the diisocyanate [HDI; Figure 10(b)] to produce a carbamate ester. Figure 15(a) shows the chemistry of this reaction. Chain extenders are required for the preparation of the polyurethane polymers. As previously shown in Chapter 2, Figure 5, the addition of chain extender diols yield linear alternating block copolymers, which are known as segmented polyurethane elastomers (Guelcher, 2008). Polymers manufactured from a copolymer chain extender (BDO.BDI.BDO) microphase separated (forming nanostructured blocks due to incompatibility) into semicrystalline hard and soft segments, and had a superior modulus (70.0 MPa) compared to those synthesized from just the BDO chain extender (23.3 MPa), likely due to the longer hard segment (Spaans et al., 2003).

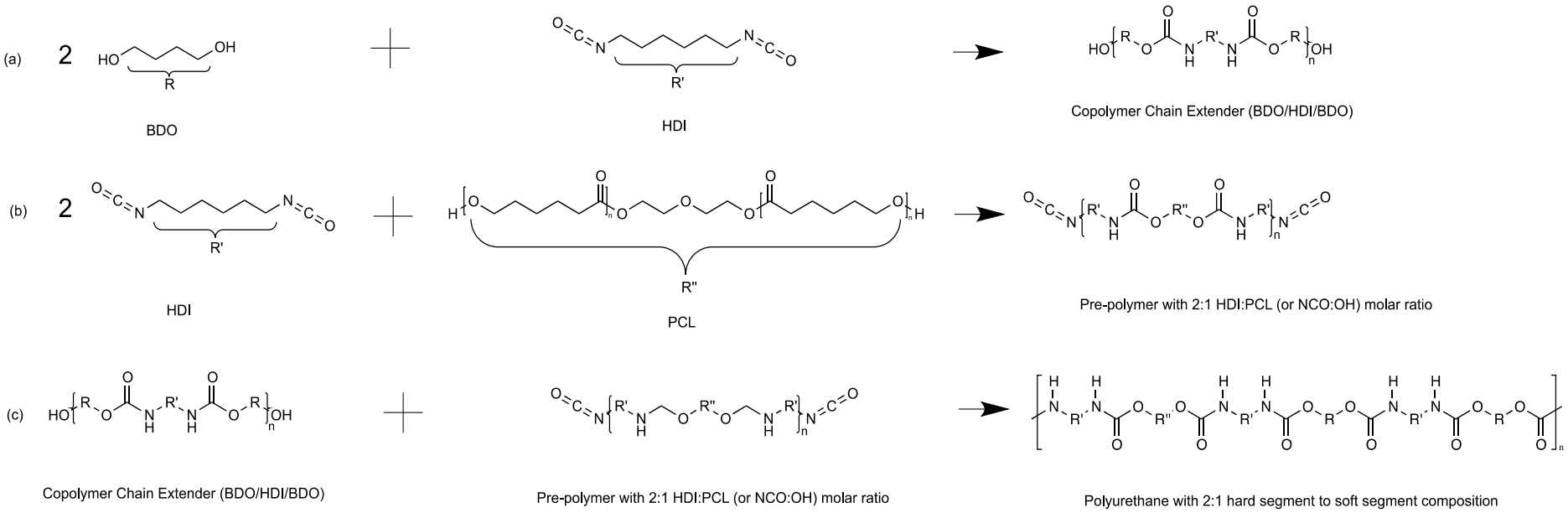

Figure 15. Synthesis of a 2:1 hard to soft segment biodegradable polyurethane with a chain extender and pre-polymer from HDI and PCL

Second step included the formation of the pre-polymer with five different molar ratios of HDI:PCL (hard to soft segments) of 1:4, 1:2, 1:1, 2:1, and 4:1. The polyol [Figure 10(c)] reacts with the isocyanate to form a urethane bond. Figure 15(b) shows the reaction between these two chemical compounds. Pre-polymers [Figure 15(b)], as described earlier in Chapter 2, offer a further level of control over the configuration of biodegradable polyurethane. The NCO-terminated pre-polymers are oligomeric intermediates with isocyanate functionality. The capability to alter pre-polymer intermediates with directed properties by changing the diisocyanate to diol ratio distinguishes polyurethanes from other polymers. The benefit of the pre-polymer method is that greater constrain can be gained over the structure and features of the polymer compared to the one-shot procedure, in which all reactants are combined immediately (Oertel and Abele, 1993). Polymers using this process have been shown to exhibit a more uniform dispersal of hard segment ratios. These even hard segments endorse improved microphase separation compared to polymers primed by the one-shot route, thus boosting the tensile modulus and strength (Spaans et al., 1998).

Third step included the final formation of the polyurethane product [Figure 15(c)] by the reaction of equal parts of the chain extender [Figure 15(a)] and the pre-polymer [Figure 15(b)]. The chemistry is dictated by the reaction of the hydroxyl-terminated chain extenders to the NCO-terminated pre-polymer in various complex combinations. Further details on this have been provided in Chapter 2.

4.2 Polyurethane Composition Characterization

FTIR spectra were recorded for the polyurethane continuous matrices of different hard to soft segment (HDI:PCL) and molar ratios of 1:4, 1:2, 1:1, 2:1, and 4:1 (Group I), to confirm the standard final compositions. Figure 16 shows five different FTIR spectra for the different samples of polyurethane with the different HDI:PCL molar ratios. This figure shows that all the samples possess the same major characteristic peaks, which demonstrates similar final composition for the five. Table 6 contains the summary of the peak assignments for the FTIR. Additionally, Table 6 correlates the peaks to polycaprolactone diol (PCL) and final polyurethane product in Figure 17. As shown in the standard FTIR spectra for HDI (not shown in this thesis), isocyanate has a characteristic band between 2250 and 2270 cm^{-1} as well as the imine (C=N) at 1635 cm^{-1} (Chan-Chan et al., 2010). Both of these peaks disappeared in the FTIR spectra in Figure 16 in the final polyurethane composition, indicating complete conversion of monomers to form polyurethane. Subsequently, the peak that arose at 1730 cm^{-1} is for the carbonyl group found in the newly formed urethane bond. Further evidence of the N-H bond present after the isocyanate reacts with the polyol (or chain extender) is through the stretching observed at 3323 cm^{-1}. The various CH_2 groups present in the system show symmetric as well as asymmetric absorbance at approximately 2864 and 2939 cm^{-1}, respectively. These values are in line with other studies where similar polyurethanes were synthesized (Hood et al., 2010). These peaks for different groups observed can be related to the chemistry of the reaction [i.e. Figure 15(a)-(c)], where the new polyurethane bonds are formed and broken.

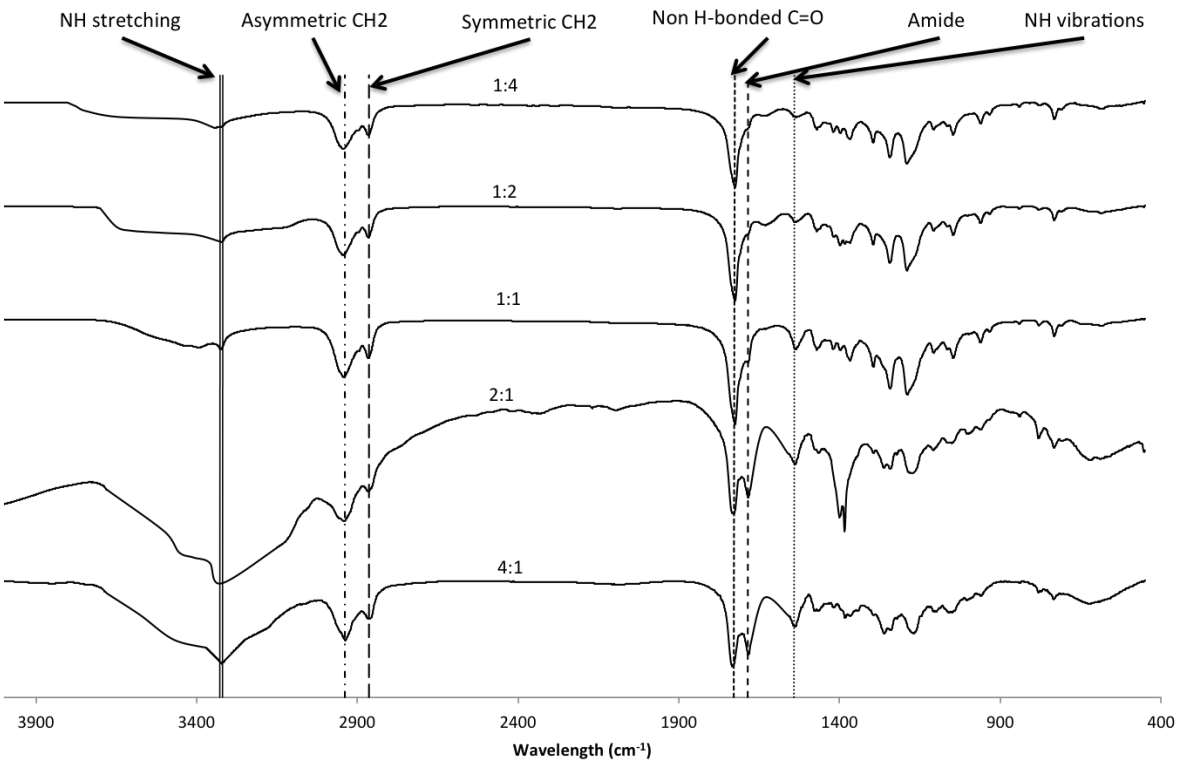

Figure 16. FTIR spectra for the five different segmented polyurethanes (Group I) with different HDI:PCL (hard to soft segments) ratios as specified on the Figure.

Furthermore, carbonyl peaks can be divided into three separate sections in the spectrum (1685, 1705, and 1728 cm^{-1}). Bands usually observed at 1705 cm^{-1} belong to the weakly hydrogen bonded N-H and C=O in the hard segment. They can also be attributed to the ester group in the soft segment of the carbamate linkage (RNCOOR). On the other hand, the peak at ~1726 cm^{-1} belongs to the non-hydrogen bonded C=O. Lastly, the amines with tough hydrogen bonds and high level of organization were observed at 1685 cm^{-1}. These carbonyls are strongly bonded with amines and exhibit curbed vibratory activities (Yilgor et al., 2006). Thus, the peak observed at 1730 cm^{-1} is attributed to non-

hydrogen bonded carbonyls and 1685 cm^{-1} to strongly hydrogen-bonded carbonyls. Hard segment content is associated with denser bonding and closely knit structures.

Table 6. FTIR peak assignments for PU samples

Wavelength (cm^{-1})	**Band Assignment**	**Figure 17 Assignment**
3323	NH stretching	G
2939	-CH_2 stretching, asymmetric	B
2864	-CH_2 stretching, symmetric	A
1728	Non-hydrogen bonded C=O	H
1685	Amide (H-bonded) (RCONHR')	I
1541	NH vibrations	G
1465, 1417, 1365, 1295	-CH_2 vibrations	-

The increase in HDI:PCL ratio amplified the intensity and broadened the peaks of the hydrogen bonded C=O at 1685 cm^{-1} as compared to their non-hydrogen bonded counterparts at 1726 cm^{-1} (Asefnejad et al., 2011). The lower degree of separation due to the higher content of hard segment shows restraint of the peak at 1730 cm^{-1}. The above trends reaffirm the results obtained by Hood et al. (2010), while measuring the morphology of polyurethanes by manipulating the hard domains. The aforementioned peaks, however, had shifted and were correlated to the 1685 cm^{-1} and 1726 cm^{-1} peaks, from literature. Understandably, there are insignificant digressions from the articles and can be attributed to the different types of soft segment and hard segment used and further to the FTIR apparatus used (Hood et al., 2010).

It was also interesting to note that the CH stretching for the polymer changed as the percentage of hard segment was modified. At 1:1 HDI:PCL (hard to soft segment) molar ratio and lower contents of hard domain, the comparative ratio of the intensity of the symmetric CH_2 peak with the asymmetric peak was higher. Consequently, as the isocyanate present was increased the ratio of the areas of the peaks at 2879 cm^{-1} to the 2939 cm^{-1} was lower.

NMR was also used to characterize qualitatively and quantitatively the final composition of the polyurethane matrices that were synthesized. Figure 17 shows a representative ^1H NMR spectrum of the sample with 1:1 molar ratio of hard to soft segment. As shown in the NMR spectrum, the spectra were calibrated by the DMSO standard peak at 2.5 ppm, and the residual peak for water was observed at 3.3 ppm (Gottlieb et al., 1997). The peaks were labeled with appropriate alphabetic assignments and were correlated to the structures of the final product. The R, R', and R'' represent the functional chains.

All mixtures contained the same peaks with minor differences in intensities. This statement is supported by the studies conducted using polyurethane compositions made of the same diol, isocyanate, and chain extender and only differing in the sequence and relative quantities (Bovey and Mirau, 1996). Additionally, it was observed that the distinctive peak for isocyanates at 3.8 ppm disappeared (Sumi et al., 1964). This confirms the formation of the final polyurethane polymer, and disappearance of the monomers with no diisocyanate remaining in the product. Table 7 shows the different chemical shifts observed with their respective assignments.

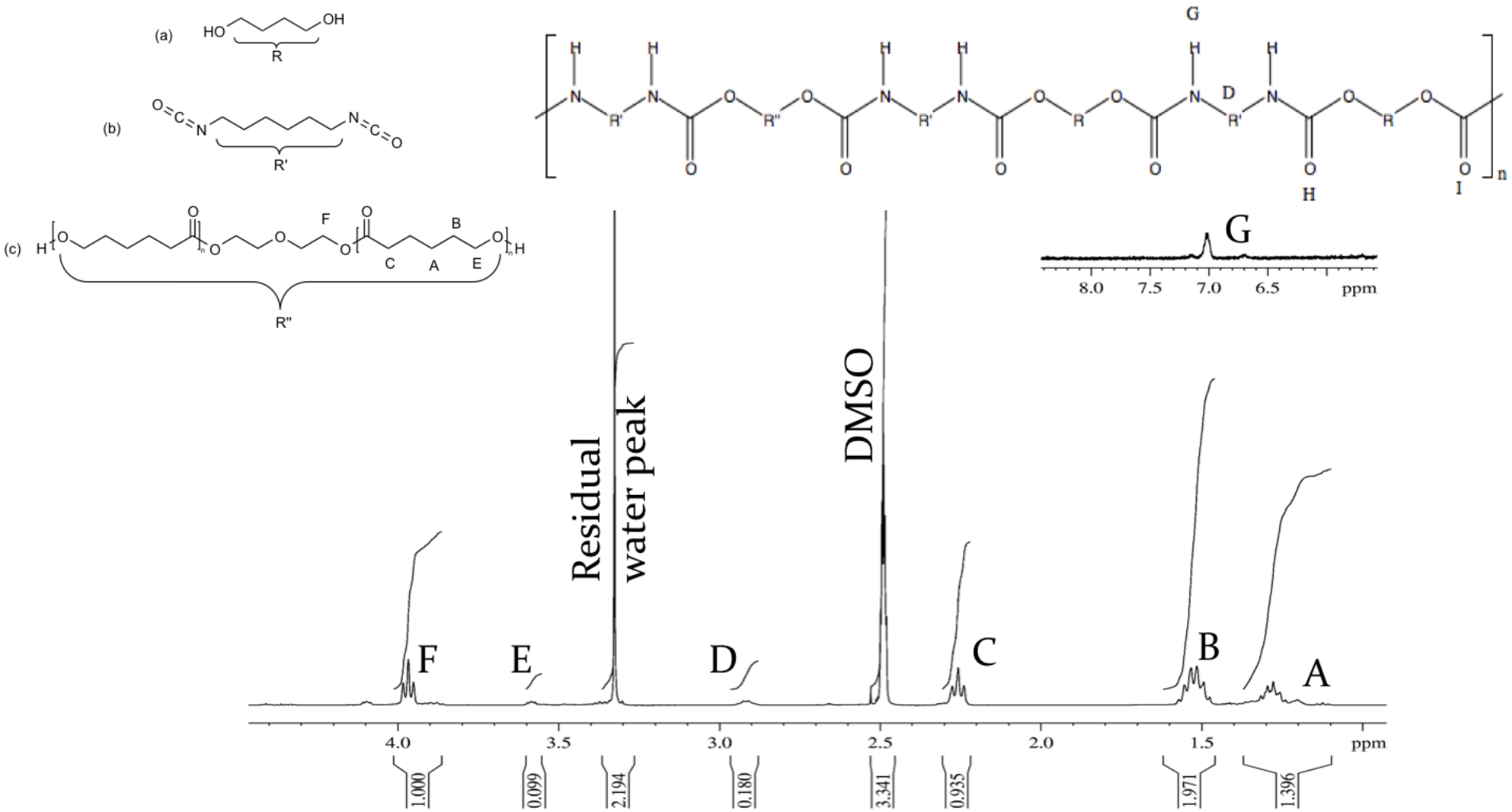

Figure 17. ^{1}H NMR spectrum of polyurethane sample with 1:1 HDI:PCL molar ratio in deuterated DMSO (DMSO-d_6)

Table 7. NMR proton peaks and assignments (Fromstein and Woodhouse, 2002; Hood et al., 2010)

Chemical Shifts (ppm)	Peak Assignment	Figure 17 Assignment
1.3	$OCH_2CH_2C\underline{H}_2$	A
1.5/1.6	$OCH_2C\underline{H}_2/OCH_2C\underline{H}_2CH_2$	B
2.25	$C\underline{H}_2CO$	C
2.5	DMSO solvent peak	-
2.9	$C\underline{H}_2NH$	D
3.3	Residual water peak	-
3.5	$HOC\underline{H}_2$	E
3.9	$OC\underline{H}_2$	F
7.0	$N\underline{H}$	G

PCL contributed to four chemically unique protons represented by: two doublets of triplets (or hextets), one at 1.3 ppm (A), and a second between 1.5 and 1.6 ppm (B), and two triplets, one at approximately 2.25 ppm (C), and at 3.9 ppm (F) (Fromstein and Woodhouse, 2002). The nitrogen elements present are representative of the isocyanate and their urethane bonds were observed on the spectra at 2.9 ppm (D) as well as 7.0 ppm (G). The labeling of peaks observed in the spectra in Figure 17 provides evidence of linear samples, with no discernible crosslinking due to allophanate bond development or other side reactions that may occur during the synthesis process (Hood et al., 2010).

The HDI:PCL (hard to soft segment) contents of the final polyurethane polymer were obtained for all samples by comparing the peaks arising from the CH_2CO (2.25 ppm) or OCH_2 (3.9 ppm) and the CH_2N (2.9 ppm) groups (Heijkants et al., 2005b;

Hood et al., 2010). Both of the carbonyl components are representative of the polyol content in the final polyurethane, which in this study was PCL. On the other hand, the unique amino group present in the hard segment was only characteristic of the reaction of HDI (Hood et al., 2010). In order to quantify the ratio of hard to soft segment in the polyurethane, the following peaks were used: CH_2CO at 2.25 ppm (dotted line), CH_2N at 2.9 ppm, and OCH_2 at 3.9 ppm (straight line). The ratio of the area of the CH_2CO peak arising at 2.25 ppm or OCH_2 peak arising at 3.9 ppm with the area of the CH_2N peak arising at 2.9 ppm was compared as practiced in literature (Heijkants et al., 2005b). Figure 18 shows the relative ratio of the HDI:PCL in the pre-polymer as compared to the ratios calculated from NMR spectra of the corresponding polyurethane samples.

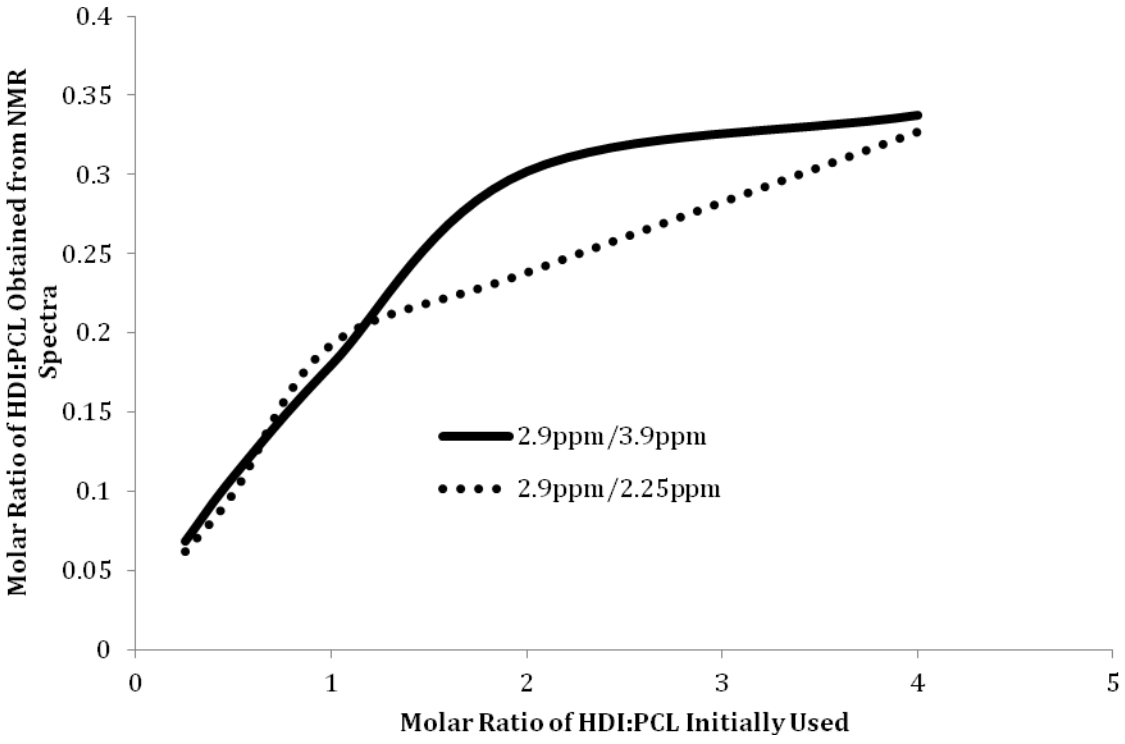

Figure 18. NMR peaks representative of initial HDI:PCL in pre-polymer

The trend in Figure 18 shows corresponding increase in the ratio of hard to soft segment that correlates with the amount used in the synthesis stage.

Although the relative amounts were calculated it was not possible to relate this to the exact structure of the polyurethane. This difficulty arises from the complex chemistry with which the different amounts of polyol and isocyanate combine with the chain extender would require various combinations and permutations to resolve. Further, the problem lies in the overlapping and similarity of functional groups belonging to different parts of the molecular structure for the compound. In similar cases of complex polymer chemistry, quantitative analysis using NMR was quite difficult and did not produce accurate results (Fromstein and Woodhouse, 2002). Interference from protons elsewhere in the polyurethane backbone, as well as proton intensities varying from sample-to-sample caused additional problems. Further analysis also showed that as increasing amounts of excess isocyanate were added, part of them were represented in the newly synthesized polymer that was characterized by NMR, and therefore there was a limit as to what would be the optimum. As seen from the graph, the slope increased with decrease in isocyanate signifying an increase in the ability of the soft domain to react with the former. The amount of isocyanate converted into the hard segment of the final polyurethane matrix depended on the initial content of hydroxylated PCL added in the pre-polymer. The lower conversion for higher hard segment contents was apparently due to the hard segment being less soluble because of its higher glass transition temperature and hence influencing the final conversion in the reaction. This limitation was observed in other polyurethane studies investigating the influence of hard segment on solubility (Xu et al., 1983).

4.3 Morphological Study of the Porous Polyurethane Using SEM

Figure 19 shows a SEM image of the porous structure of the polyurethane sample synthesized with 1:2 HDI:PCL (hard to soft segment) molar ratios without the reinforced nanofibers. The porosity and interconnectivity of the scaffolds was evident through the pictures. It was also observed that the final pore size was in the range of 125-355 µm with interconnected channels. This allows the cells to infiltrate the holes and grow on the thick surface and walls.

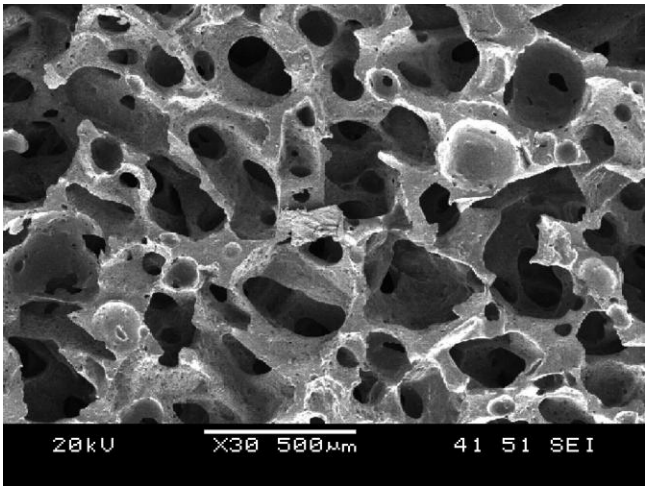

Figure 19. SEM image of porous polyurethane sample that was synthesized with 1:2 molar ratio (HDI:PCL); (Group II)

Figure 20 shows a more focused SEM image of a regular pore in the polyurethane sample synthesized with 2:1 HDI:PCL stoichiometric ratio, reinforced with 5 wt% BCNF. The size of the pores was ascertained to be between 125-355 µm. These regular, homogeneously dispersed apertures correspond to the size of insoluble NaCl crystals used while salt leaching. The solvent casting and salt leaching method had the benefit of managing the pore dimensions by controlling the size of the porogen. Nevertheless, the

ensuing scaffold may have inadequate interconnectivity, which would unfavorably influence cell seeding and proliferation (Guan et al., 2005). Hence, the simultaneously run thermally induced phase separation method may be attributed to producing smaller pores ranging from 10 µm to 50 µm.

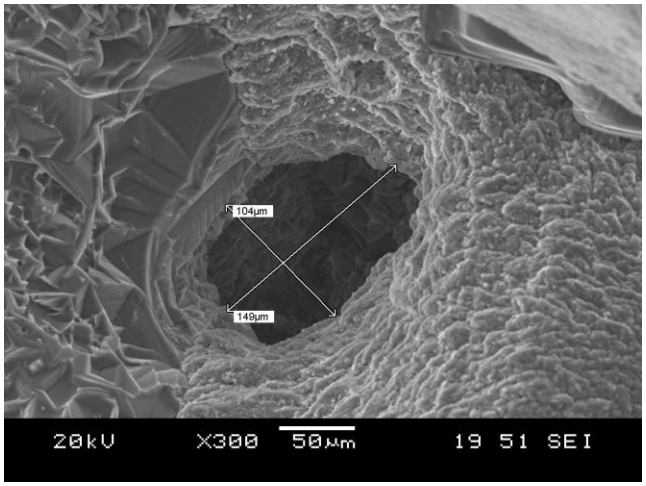

Figure 20. SEM image of a pore in a 2:1 molar ratio (HDI:PCL) biodegradable polyurethane scaffold with 5 wt% biocellulose nanofibers (Group III)

Similarly, Figure 21 shows a SEM image of the porous structure and interconnectivity of the polyurethane sample synthesized with 1:4 HDI:PCL (hard to soft segment) ratios. The addition of the small quantity of DDI water, used as a nonsolvent, decreased the solvent quality. This proportionally stimulated liquid-liquid phase separation and consequently the increase in water content increased the level of interconnectivity observed. A polymer-rich phase and a polymer-lean phase were created using the non-toxic DMSO, with the polymer-poor phase located around the NaCl crystals. This polymer-lean phase wets the salt crystals, forming polymer-poor bridges and leads to the interconnected pores (Heijkants et al., 2008). The amount of crystallized

solvent decreases with an increase in water concentration, thus a balance needs to be achieved between the two agents of interconnectivity.

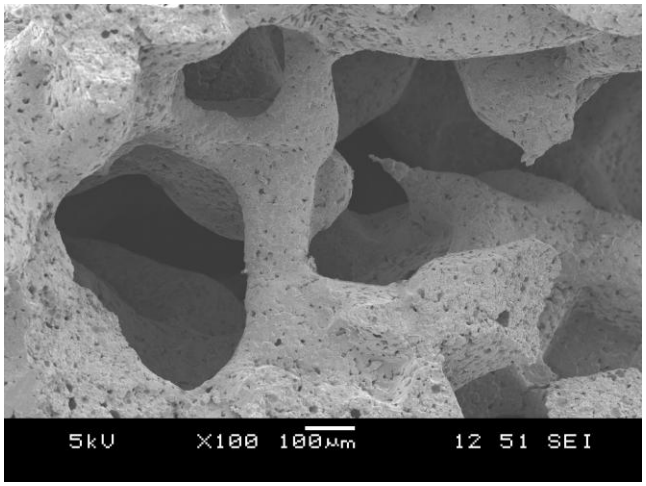

Figure 21. SEM image of interconnectivity in 1:4 HDI:PCL (hard to soft segment) molar ratio porous polyurethane product (Group II)

The polymer concentration also dictates the level of interconnectivity and the amount of ineffective pores, but hampers the homogenous mixing of the salt and nonsolvent (Heijkants et al., 2006). The foam structure confers adequate porosity that may induce cell attachment as well as vascularization for the appropriate ingrowth of tissue. Figure 22 shows a SEM image of the porous structure and smaller pores of the polyurethane sample synthesized with 1:1 pre-polymer HDI:PCL ratio and reinforced with 5 wt% green nanofibers.

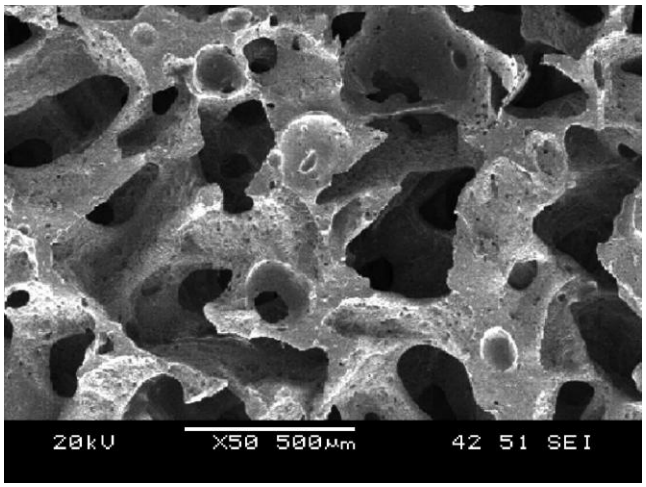

Figure 22. SEM images of reinforced (5 wt%) polyurethane with 1:1 molar ratio (HDI:PCL); (Group III)

Further magnification was required to show the fibers of smaller sizes to examine the reinforcement of nanofibers within these polymer scaffolds. Figure 23 shows these nanofibers incorporated into the polyurethane matrix with a 5 wt% concentration. The full integrity of the nanofibers in the continuous matrix of the polyurethane, which acted as supporting mesh to the final structure, was also observed.

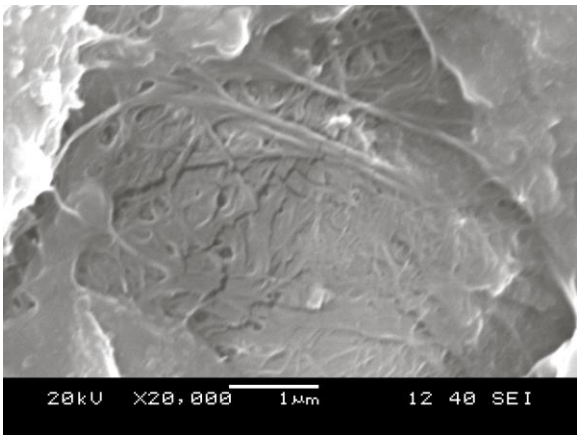

Figure 23. Nanofibers visible in 5 wt% reinforced scaffold, 4:1 HDI:PCL (hard to soft segment) molar ratio, observed through SEM (Group III)

Moreover, studies also suggest that fibers may channel the pores as they shape and aid in breaking through the barrier of the pores, in so increasing the interconnectivity of the scaffold (Slivka et al., 2001).

Porosity of all final composite samples that was calculated using the liquid displacement method, showed generally higher numbers as predicted by previous reports (Heijkants et al., 2004). Porosity ranged between 57-75% with a trend of decrease in HDI:PCL content leading to a higher pore content. This was probably caused by the hydrophobic soft domain, which repels more salt dissolved water compared to the polar hard domain. This also correlated to common decrease in mechanical strength as the porosity increased, which was typical while investigating porous composites in tissue engineering.

Further, it was observed from Table 8 that scaffolds with reinforcement showed lower porosities when compared to the ones without. Non-reinforced products had porosities between 70-75% whereas those that were reinforced with 5 wt% nanofibers had porosities between 64-70% and those with higher degrees of reinforcement had pore content between 57-69%. This may be accounted to the fact that nanofibers were most likely positioned within the 125-355 µm pores as well, and hence occupy additional space making the scaffold fully dense (Xu et al., 2001). Apart from the penetration of cells, the porosity also helps with the bulk degradation of the scaffold, which was important when considering the final application of the scaffold as an implant that has potential to be used to replace load-bearing tissue.

Table 8. Mechanical properties and porosities of polyurethane matrices

		Pre-polymer HDI:PCL Ratio				
		4:1	**2:1**	**1:1**	**1:2**	**1:4**
Basic Polyurethane Matrices (Group I)	Compressive Strength (MPa)	19.63	18.48	4.95	2.38	2.06
	Tensile Strength (MPa)	10.4	9.44	5.58	4.61	2.02
Porous Polyurethane Matrices (Group II)	Compressive Strength (MPa)	0.89	0.68	0.33	0.15	0.13
	Tensile Strength (MPa)	0.61	0.53	0.32	0.2	0.09
	Porosity (%)	70.5	71.4	72.7	73.9	75.0
Biocomposite Samples (5 wt%) (Group III)	Compressive Strength (MPa)	1.64	1.16	0.55	0.21	0.20
	Tensile Strength (MPa)	1.31	1.13	0.53	0.29	0.14
	Porosity (%)	64.7	64.2	66.6	70.0	68.0
Biocomposite Saples (10 wt%) (Group IV)	Compressive Strength (MPa)	-	1.5	0.7	0.3	-
	Tensile Strength (MPa)	-	1.29	0.67	0.39	-
	Porosity (%)	-	59.4	60.7	69.3	-
Biocomposite Samples (15 wt%) (Group IV)	Compressive Strength (MPa)	-	0.23	0.04	0.12	-
	Tensile Strength (MPa)	-	0.31	0.25	0.09	-
	Porosity (%)	-	57.0	58.7	69.0	-

4.4 Mechanical Properties of the Polyurethane Scaffolds

The mechanical properties play a central role in the formation of tissue and supporting the matrix when the tissue is growing (Hutmacher, 2000). Bone undergoes squeezing due to its load bearing function and calcium salts help to strengthen these properties. Compression testing assists in discovering the significant pressure at which materials that need to replace bone would get crushed. Collagen fibers in the bone aid in their stretching properties, although the muscles endure most of this function. Tensile testing helps in determining the force the materials can undergo before they tear apart. The tensile strength is important in the bone because it aids in absorbing the various compression forces that impact them, much like the cables in bridges sway back and forth (Larry Trivieri, Jr.). This flexible nature maintains the overall structure and foundation without which the bones would soon weaken and eventually collapse. Against this background, the compressive and tensile strengths of the different composite samples with varying compositions (hard to soft segment ratios in addition to reinforced nanofibers contents) were examined.

4.4.1 Compressive Testing

Figure 24 shows results for the compressive strength of the basic nonporous polyurethane matrices with different HDI:PCL molar ratios (Group I in Table 8). As shown in Figure 24, it was observed that compressive strengths linearly decreased when the hard domain content declined. The maximum compressive strength achieved was 19.63 MPa when the hard to soft segment ratio (i.e. HDI:PCL) was maintained at 4:1. The compression strength dramatically decreased to 2.06 MPa when HDI:PCL was 1:4

(see Table 8). From the analysis of the results in Figure 24 it was observed that as the HDI:PCL content increased, the compressive properties grew more rapidly. As shown in Figure 24, the increase in compressive strength was constant until the 1:1 molar ratio of HDI:PCL in the basic polyurethane matrix (Group I).

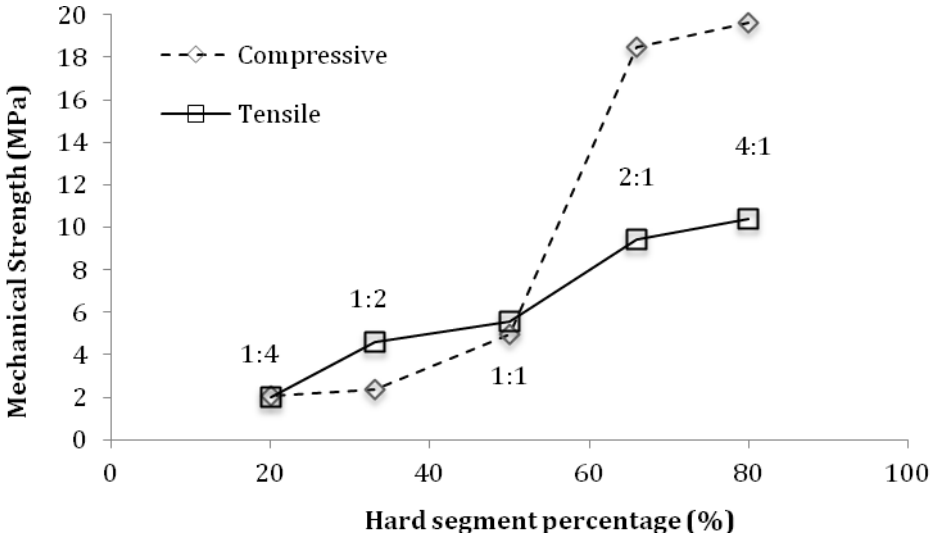

Figure 24. Mechanical properties of basic polyurethane matrices (Group I) with different HDI:PCL ratios

However, as the hard segment content increased to 2:1 (i.e., molar ratio of HDI:PCL) the increase in strength was comparatively more drastic. Similar trend of marked increase in compressive strength when hard segment was increased, was also observed in several previous studies (Petrović et al., 1998; Gorna and Gogolewski, 2003; Guelcher, 2008). Apparently the soft domain fraction acted as the continuous phase at low hard segment content. In this case, aggregation of hard segments takes place to form hard domains that provides reinforcement as fillers and formed physical crosslinks within this matrix. However, when the hard segment content was increased, it comprised the

continuous phase and inter-connected hard domains were produced, with soft domains toughening the material (Bengtson et al., 1985; Korley et al., 2006).

Figure 25 shows the changes in compressive strength of the porous polyurethane matrices with different HDI:PCL molar ratios (Group II in Table 8) As scaffolds were made porous, mechanical properties drastically decreased to approximately 5% of the original product. This phenomenon is considered as one of the main challenges related to the tissue engineering industry when fabricating porous scaffolds as discussed earlier in the literature review (Karageorgiou and Kaplan, 2005). Examining Figure 25 shows that the trend of increase in hard segment with respect to the soft segment was similar to the previous model. However, the increase in strength was less rapid once porosity was introduced.

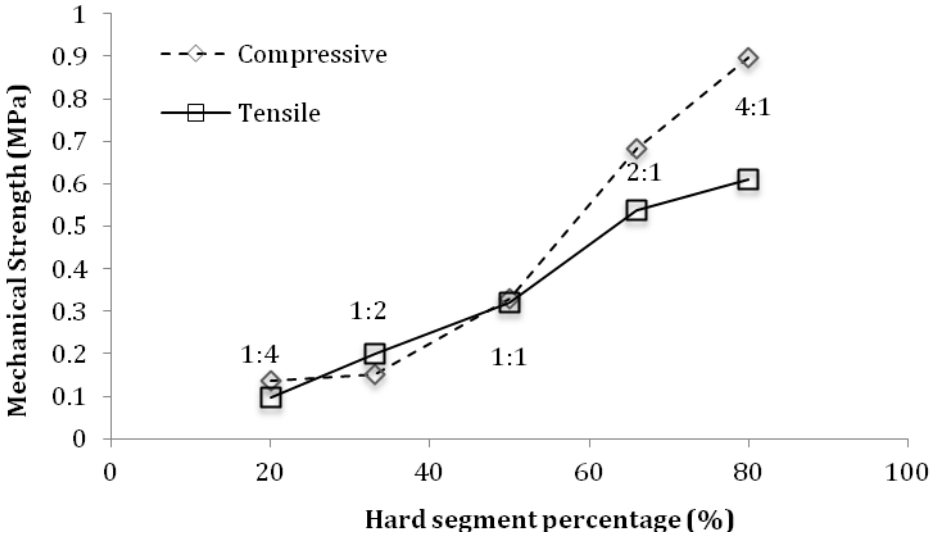

Figure 25. Mechanical properties of porous polyurethane matrices (Group II) with different HDI:PCL ratios

This can be seen in the 2:1 HDI:PCL molar ratio of porous polyurethane sample, which may be attributed to the porosity impacting the integrity of the hard segment more than the soft (Coury et al., 1988). Generally, porous samples of polyurethane matrices (i.e. Group II) exhibited compression strengths ranging from 0.13-0.89 MPa (see Table 8).

Next, scaffolds that had been reinforced with BCNF were measured. The comparative compressive strengths were analyzed for the biocomposite samples with 5 wt% BCNF reinforcement with different HDI:PCL molar ratios as listed in Table 8 (Group III). Figure 26 shows the change in the compression strength for the different composites reinforced with 5 wt% of nanofibers. As shown in this Figure, the trend showed a larger increase in strength for hard segment (4:1 HDI:PCL molar ratio of biocomposite scaffold) but both phases were impacted.

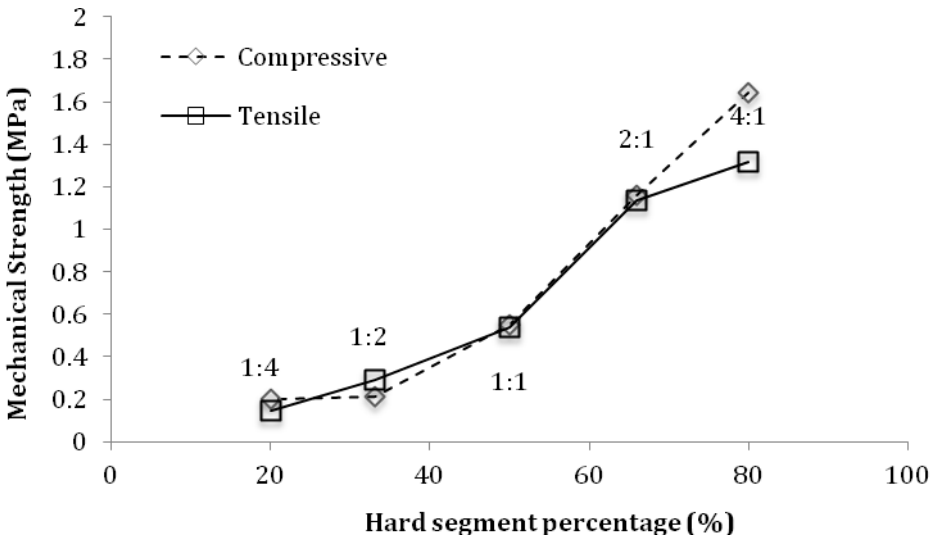

Figure 26. Mechanical properties of 5 wt% biocomposite samples (Group III) with different HDI:PCL molar

In Figure 27, compressive strength showed significant improvement after the polyurethane porous samples (Group II) were reinforced with the nanofibers at 5 wt% content. Compressive strength ranged from 0.20-1.64 MPa (Table 8) with the increase in strength of 55.6%, 40%, 66.7%, 70.5%, and 82.5% of the original porous polyurethane matrices (Group II) for 1:4, 1:2, 1:1, 2:1, and 4:1 molar ratios of HDI:PCL respectively (porosity was constant between 64-70%), which shows that the strength almost doubled. It was observed that polymers that had lower HDI:PCL (hard to soft segment) ratios showed a minor increase in strength as compared to their higher HDI containing counterparts. This phenomenon may be attributed to the ability of hydrophilic diisocyanates in the hard segment to form stronger covalent bonds with the hydroxyl group laden surfaces of the BCNF. This validated the fact that the hydrophobic soft domain was not as accommodating to the polar nanofibers as the hard domain (Wan et al., 2009). Further, the preferential interactions of the reinforcing agents with polyurethane hard segments led to a transfer of stress from these hard domains (that usually bear these stresses) to the reinforcing agents. In polyurethanes that contain higher concentrations of soft segment, the soft domains accommodate lower quantities of reinforcing agents. In contrast with polyurethanes that contain higher concentrations of hard segment and their soft domains can accommodate higher concentration of reinforcing agents as observed from a previous study (Fernández-d'Arlas et al., 2011). Moreover, it is known that the hard domain plays a more important role in dictating the mechanical properties; hence their reinforcement would show superior effects on the properties of the material.

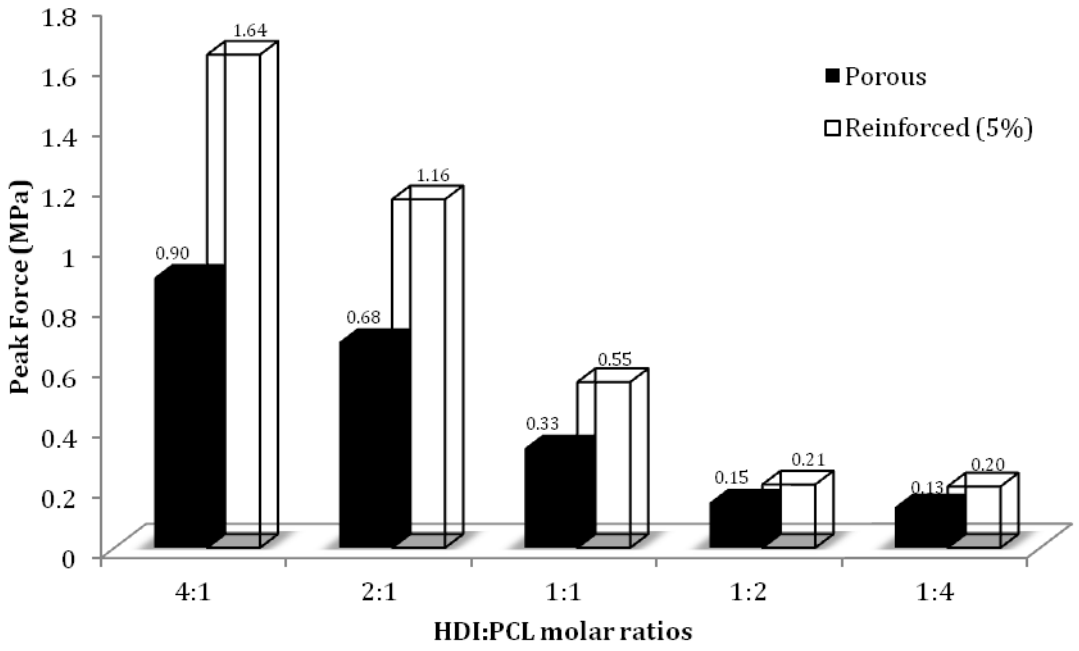

Figure 27. Compressive strengths of porous matrices and biocomposite scaffolds with 5 wt% BCNF (Groups II and III)

4.4.2 Tensile Testing

Similarly, Figure 27 shows the tensile strength of the nonporous polyurethane polymer follows a linear trend with respect to the amount of isocyanate and polyol in the blend (Group I in Table 8). As the HDI:PCL molar ratio increases the tensile strength increases, with the highest being 10.4 MPa (4:1 HDI:PCL molar ratio in Group I; Table 8). A low tensile strength of 2.02 MPa was observed with 1:4 ratio of HDI:PCL (hard to soft segment) and significantly increased thereafter in Figure 27. The flexibility of the soft domain versus the rigidity of the hard domain is of significance when discussing these mechanical properties. It is known that the hard segment adds fortification to the polymer, resulting in proportional strength (Crawford and Teets, 1997). Aparently, the increase in intramolecular pull amongst hard and hard segment due to the hydrogen

bonding between –NH and –C=O of hard segment causes a subsequent increase in stress. The increase in Hydrogen Bonding Index (HBI) increases the phase mixing, strength, and decreases strain with respect to the diisocyanate content (Huang and Lai, 1997).

Figure 25 shows the comparative assessments in the previous subsection in which analogous tests were run after porosity was induced in the prepared polyurethane polymers. It was evident that the properties diminished, in some cases as much as 95.6% (1:2 HDI:PCL molar ratio in porous polyurethane matrix of Group II), once again showing the influence of porosity on mechanical properties. This is common while investigating scaffolds in this industry, as once porosity is induced a large part of the mechanical properties diminish as compared to the non-porous composites. Porous polyurethane matrices showed tensile strengths up to 0.61 MPa (in 4:1 HDI:PCL molar ratio) but reduced as the hard segment content is decreased (Group II in Table 8).

Figure 26 shows the tensile strength for 5 wt% cellulose nanofiber reinforced scaffolds with varying isocyanate and polyol ratio. As seen from Table 8, much like the compressive analysis, the improvement in tensile strength was manifested in all different samples. The increase in strength with different concoctions may be visualized in Figure 28 below. The tensile strengths observed in the range of 0.14-1.31 MPa (1:4 and 4:1 HDI:PCL molar ratio in biocomposite scaffolds of Group III) may be compared to the strengths of cancellous and smaller bones (higher than 0.12 MPa) and hence have applications as their scaffolds (Table 8).

It is interesting to note that the hard and soft domains play a role in the mechanical properties of the novel reinforced scaffolds. When only 5 wt% of BCNF was

added, it showed a 115.6%, 113.2%, 65.6%, 45%, and 50.5% increase of the original porous polyurethane matrices (Group II) for 4:1, 2:1, 1:1, 1:2, and 1:4 HDI:PCL molar ratio (hard to soft segment ratio) amalgam (porosity was constant between 64-70%), which shows that the strength doubled in some cases as seen from Table 8. This supports the initial hypothesis that the hard segment was better able to support the reinforcement as compared to those polymers that were low in hard segment. The polar groups of cellulose interact with the relatively polar hard domains of the polyurethane leading to good interfacial adhesion, which is essential for enhanced mechanical properties (Siró and Plackett, 2010).

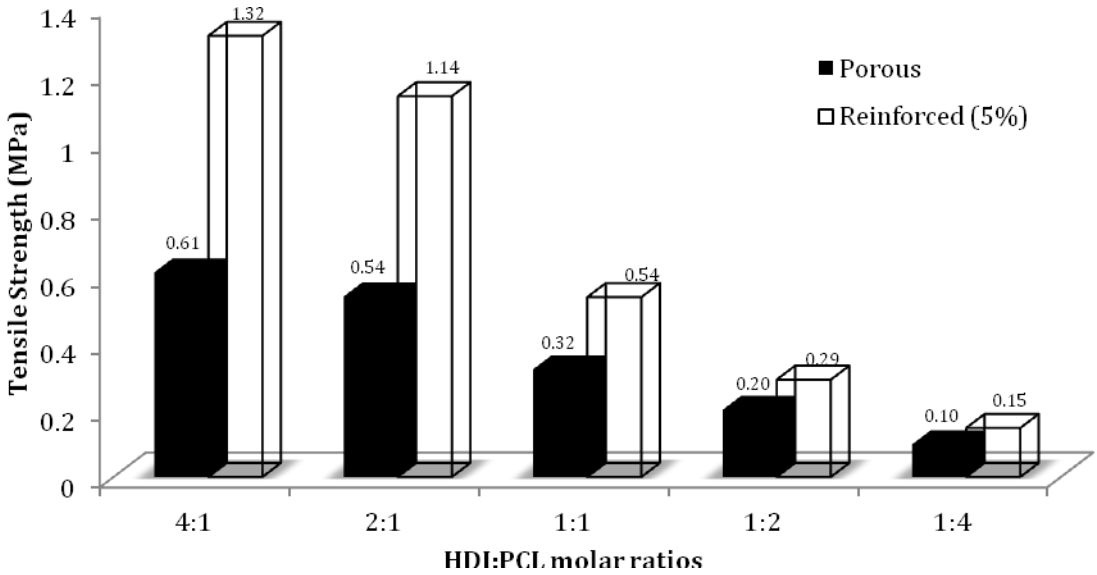

Figure 28. Tensile strengths of porous matrices and biocomposites with 5 wt% BCNF scaffolds (Groups II and III)

There was a slight inconsistency in the increase in strength with respect to the HDI:PCL (soft segment to hard segment) ratios as 1:4, for both compressive and tensile

strengths, showed more improvement than 1:2 molar ratio (Table 8). The similar unexpected results led to the inference that while preparing the 5 wt% reinforced 1:2 mixture (Group III) there was an error, likely due to insufficient nanofiber addition. It is also noteworthy to report that from Figures 27-29, the trend for increase in tensile strength was fairly linear regardless of hard segment content, which represents a lack of correlation with factors such as porosity.

4.4.3 Effect of Nanofibers Contents on Tensile and Compressive Strengths

Attracted by the significant find that 5 wt% of BCNF enhanced the strength of the prototype, the effect of increasing reinforcement content on the aforementioned attributes was researched. Hence, the same testing was repeated for scaffolds that were reinforced with 10 wt% and 15 wt% BCNF. The compressive strength of the 10 wt% showed substantial increase of 100%, 112.1%, and 119.5% of the initial porous polyurethane matrices (Group II in Table 8) for 1:2, 1:1, and 2:1 molar ratios of HDI:PCL respectively (porosity was constant between 59-70%), which shows that the strength more than doubled. Figure 29 shows the strength, which does not increase proportionally as compared to the 5 wt%. Interestingly enough, all the 15 wt% samples did not show any increase in strength, and as a matter of fact lessened the initial strength of the material. This might be because at such high weight content of reinforcing agent the scaffold disintegrates. This degree of nanofiber reinforcement, does not allow for a complete matrix to be formed between the two phases. At this point the nanofibers are impeding the structural bonds of the hard and soft domains and allowing it to succumb to stress, as further described below.

The compressive strength of 1.5 MPa observed in the reinforced scaffolds needs to be further enhanced for use in applications with hard tissue as shown in Table 1. The increased reinforcement tests that were run on the samples with 2:1, 1:1, and 1:2 stoichiometric pre-polymer HDI:PCL molar ratios (Group IV) were compared in Table 8. The porous material that had no BCNF was used as the base reference and used to calculate the percentage change in strength.

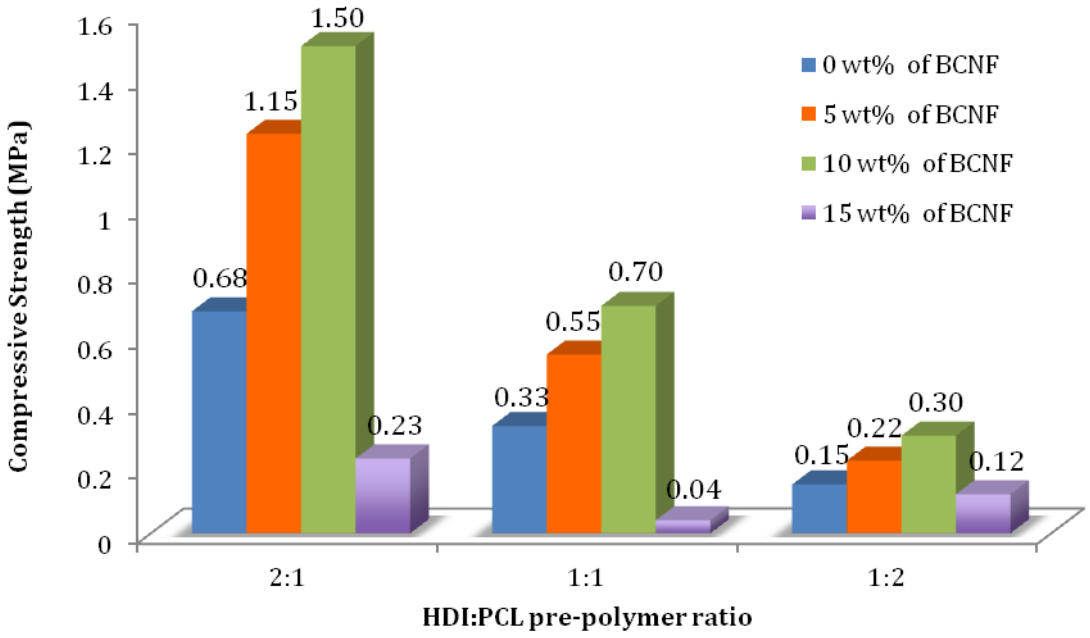

Figure 29. Reinforcement influencing the compressive properties of 2:1, 1:1, and 1:2 molar ratio of HDI:PCL porous polyurethane product (Groups II, III, and IV)

Table 8 shows the results for the tensile tests that were conducted on the green polyurethane scaffolds with 10 wt% and 15 wt%. The use of the three different HDI:PCL molar ratios and their consequent effect on the mechanical properties were highlighted in Figure 30. The samples with 10 wt% were able to withstand higher stress before they

failed, but not to the extent as the 5 wt% reinforced scaffolds previously had. The percentage increase in tensile strength ranged from 96.5%, 109.4%, and 140.5% of the initial porous polyurethane matrices (1:2, 1:1, and 2:1 HDI:PCL molar ratios in biocomposite scaffolds of Group IV), with the polymers with higher hard segment showing better improvement (porosity was constant between 59-70%), which shows that the strength more than doubled as seen from Table 8.

A study using cellulose nanocrystals (CNC) to reinforce waterborne polyurethane with 0-30 wt% in 5% increments, showed comparable results. With 5 wt%, the tensile strength increased from 4.3 MPa to 9.3 MPa but the 10 wt% showed only an increase to 10.2 MPa. It was claimed that the phenomenon can be explained by the fact that a rigid filler network is formed as the CNC content increases and is responsible for this unusual enforcing effect (Cao et al., 2007). The addition of more reinforcing agent does not add value to the already produced filler network. By reaching this percolation point (threshold for filler movement) it was plausible that no matter how much nanofiber was enforced, it would not be able to enhance the materials strength.

In Figure 33, similarly, the tensile properties of the scaffolds containing 15 wt% nanofibers showed decreased strength. This supports the fact that there was a threshold as to how much BCNF reinforcement the novel polyurethane biomaterial can absorb. It was hard for the scaffold to hold its structure once a significant amount of reinforcing agent was added. This can further be explained by considering the fact that after an evident tension value, nanofibers begin slipping. Stress was concentrated at points close to where this slippage occurs. This leads to a fracture being spread and the nanocomposite can no longer provide the original stiffness (Fernández-d'Arlas et al., 2012). After the

percolation limit, the higher the nanofiber content, the more the slippage points would be detected. These crack propagating locations deter the initial strength of the polymer rather than reinforce it.

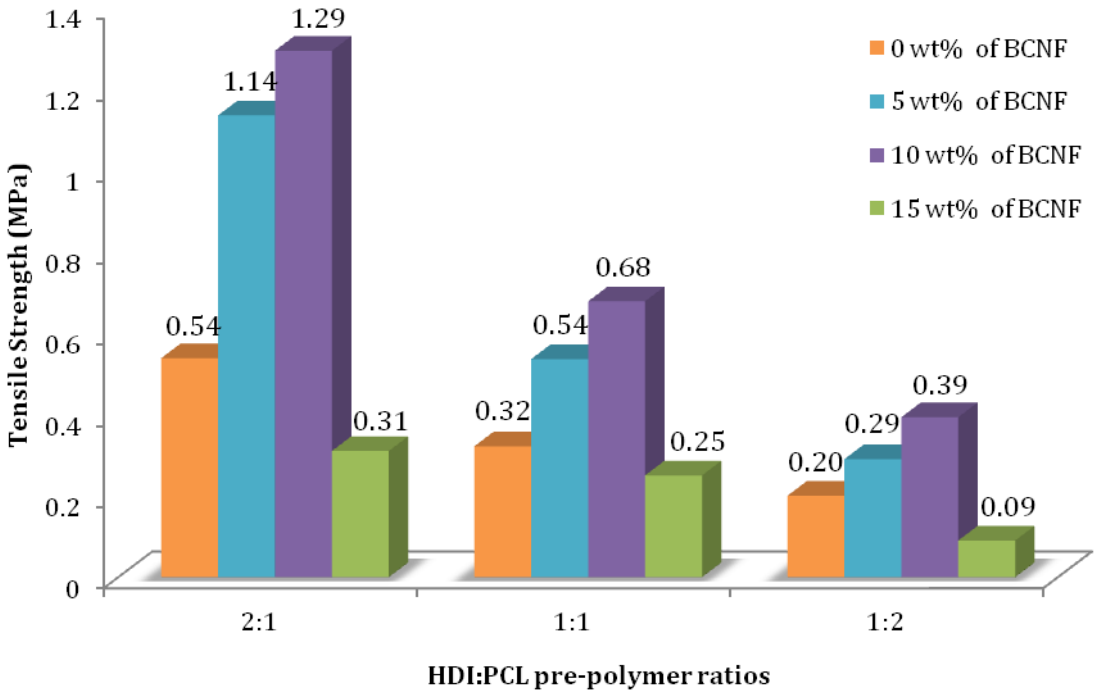

Figure 30. Increase in biocellulose nanofiber wt% reflected on tensile strength on porous polyurethane with 2:1, 1:1, 1:2 molar ratio of HDI:PCL (hard to soft segment); (Groups II, III and IV)

4.4.4 Temporal Profile of Polyurethanes of Different Compositions (Group I)

The melting temperature of polyurethane polymer was substantially influenced by the amount of isocyanate and polyol. The approximate temperature at which the solid polymer transitions to a highly viscous, gel-like substance was measured. Figure 31 illustrates how the increase in hard segment content resulted in an increase in melting

temperature. The miscibility increased in the polymers with higher HDI:PCL contents, and the hard domain confined the movement of the soft domain as the former was dispersed into the latter. This supported the fact that phase separation decreased as the HDI:PCL ratio was increased (Sánchez-Adsuar et al., 1998).

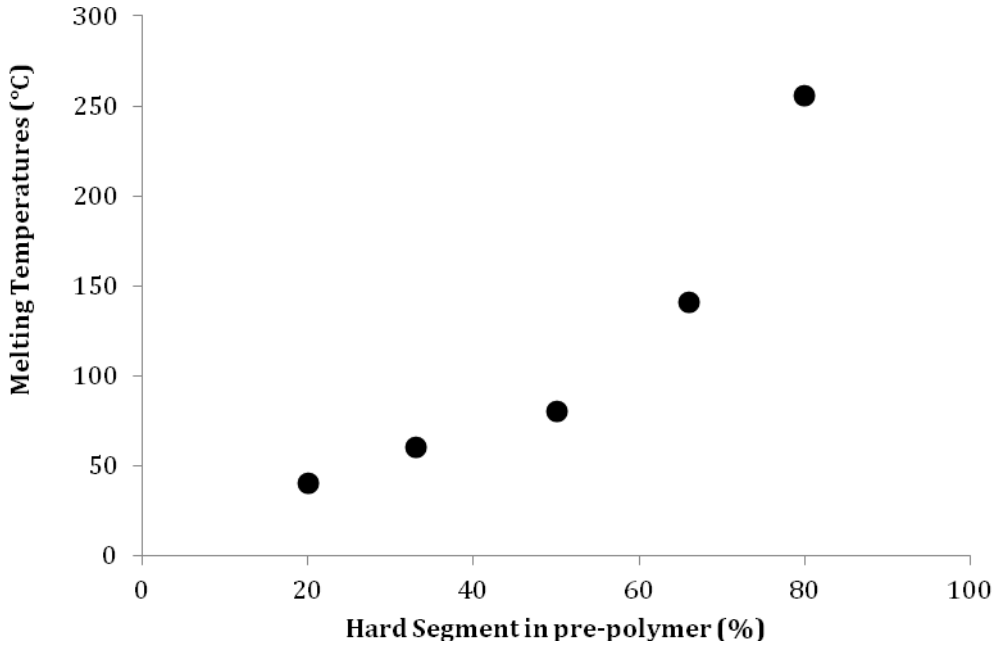

Figure 31. Melting temperature of different polyurethane polymer samples (Group I) as a function of composition

In summary, results from the present study confirm the ability to tailor the composition of the novel polyurethane through manipulating the hard and soft segment ratios (i.e., HDI and PCL). Mechanical properties were found to increase proportionally with the increase in hard segment content. Results also demonstrated the ability to improve the mechanical properties (compression and tensile strengths) of the porous polyurethanes composites through the addition of biocellulose nanofibers. The addition

of green biocellulose nanofibers has led to an increase in the mechanical strengths of the novel scaffolds up to a certain threshold to curb the detrimental effects of inducing porosity on tensile and compressive properties. These biodegradable and biocompatible polymers carry potential to be used in the regenerative medicine of smaller bones like the iliac crest and soft tissue. Through varying the ratio of preliminary constituents or the extent of reinforcement, final composite mechanical properties can be tailored to mimic properties of specific tissue.

CHAPTER 5

CONCLUSION AND FUTURE WORK

5.1 Conclusion

Results in the present work demonstrated the effect of the final composition of polyurethane based biocomposite on the mechanical properties. Biodegradable polyurethane scaffolds composed of HDI, PCL in addition to BDO/HDI/BDO as chain extender were synthesized. A total of 21 different samples were produced which were divided into four different groups: Group I represents basic polyurethane matrices with 5 different compositions of HDI:PCL molar ratio. FTIR and NMR were used to characterize all five blends and the change in ratios was confirmed during analysis. Group II signifies developing the porous structure in the polyurethane matrices with 5 different compositions from Group I. Interconnected pores were introduced to the molds using a combination of salt leaching and TIPS. Group III comprise the composite scaffolds that were reinforced with 5 wt% biocellulose nanofibers with 5 different initial hard to soft segment compositions from Group II. Lastly, Group IV encompasses 3 of the 5 polyurethane polymer compositions from Group III with enhanced reinforcement contents of 10 and 15 wt% BCNF.

Mechanical testing was carried out using ASTM E8 standards to analyze tensile and compressive strengths. Increase in the HDI:PCL molar ratios (or hard segment content) showed greater compressive and tensile strength throughout the five different polyurethane compositions in Group I. A porosity between 70-75% led to a reduction of almost 95% being observed in both mechanical properties in Group II. Consequently, the

reinforcement using novel biocellulose nanofibers enhanced the mechanical properties to a little bit less than two-fold (between 55-114% increase for tensile strength and by virtually 53-85% for compressive strength) for 5 wt% reinforcement (64-70% porosities) compared to the porous polyurethane matrices (Group III in Table 8). The increase in nanofiber content also showed a corresponding augmentation in strength with 10 wt% BCNF increasing the compressive strength of the sample to more than two-fold (compressive by 100-120% and tensile strength between 95-140%; 59-69% porosities) of the porous polyurethane matrices (Group IV in Table 8). This was true up till an evident saturation point (15 wt% BCNF with 57-69% porosity). Further, a trend was observed in the ability of the polyurethane blend, depending on its specific composition (HDI:PCL molar content), to attract nanofibers and accordingly show superior properties measured up against its lower hard segment content counterparts.

From an economic standpoint, nanocomposites that are attained from the green nanofibers that was synthesized from agriculture residues may possibly be employed for surrogating polyurethanes with high hard segment matter, therefore generating low-cost materials because of the reduction of diisocyanate monomer.

The unique control over tensile and compressive strengths (relating to porosity) as well as potential biodegradability for these biocompatible polyurethanes has sparked interest for use in medical applications after further R&D. Even though the values achieved in this study are superior to those reached in most comparative biodegradable scaffold studies, the application towards hard tissue, like bone, cannot be justified. However, relevance towards softer tissue, like cartilage and ligaments are valid and further improvements could lead to better applicability.

5.2 Future Recommendations

It is recommended to further measure the modulus of the synthesized samples to examine the effect of reinforced nanofibers. This measurement would add support to the fact that based on strain the material could observe complementary properties to different tissues. It is also recommended to measure the molecular weight and the molecular weight distribution of the synthesized polyurethane samples. Furthermore, Differential Scanning Calorimetry (DSC) needs to be conducted to analyze the effect of the composition on the melting and glass-transition temperatures of the novel composite. It is strongly recommended to synthesize and test cross-linked samples based on the same recipe.

For use in regenerative medicine and even as drug delivery vehicles, the biodegradation rates of the composite samples need to be analyzed. It is known that the polarity of the hard and soft segments dictates the hydrolysis rate and gives rise to degradation products (Santerre et al., 2005). These breakdown substances have acidic characteristics that might be beneficial to quantify based on pH. Calculating the mass loss in a given period of time is also an interesting method of analysis. It might also be advantageous to improve the chain extender into one that is biodegradable like the diisocyanate and the polyol.

The next step would be to introduce the scaffold to an in vitro cell culture and quantify the seeding and attachment of cells on its surface. Also, the product needs to undergo in vivo animal testing and later clinical studies for cytotoxicity and biocompatibility investigations.

The reinforcement material, in our case the biocellulose nanofibers, could themselves be modified to offer more attractive surface chemistry that might aid in the attachment with the scaffolds. Apart from an increase in compressive strength, functionalization has also increased cell viability (Cunningham and Veenis, 2010). Our research group is currently conducting studies on the controlled modification of biocellulose nanofibers by grafting poly(hydroxyethyl methacrylate) and tailoring its polarity.

Furthermore, the aspect of growth factors like bone morphogenetic proteins (BMP-2 that has been approved by the FDA) has not fully been understood, but is definitely promising in tissue engineering for cell differentiation and proliferation (Saito and Takaoka, 2003). Coalescing biocompatible and biomechanically fitting scaffolds with osteogenic cells (MSCs or osteoblasts) or a bone growth stimulating agent may boost the treatment of defects, devoid of autografts and allografts, and present themselves as medical substitutes for bone restoration (Reichert et al., 2011).

Other materials such as hydroxyapatite and calcium phosphate have also been used primarily for calcification of bone and strength, opening the gateway to osteoconductive, osteoinductive and even osseointegrative implants (Albrektsson and Johansson, 2001). With apt materials, the structure, and eventually even the functionality of bone could be mimicked, creating the potential to regenerate osseous tissue, and change the face of orthopedics forever.

APPENDICES

Appendix A: NMR Spectra of the different Polyurethane Samples

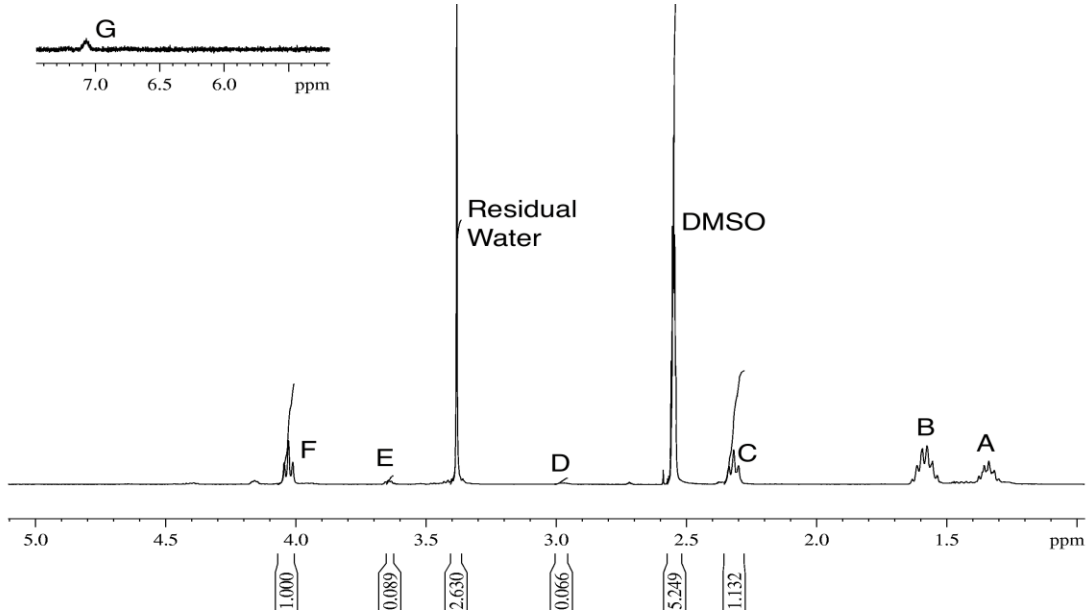

Figure 32. ^{1}H NMR spectrum of polyurethane sample with 1:4 HDI:PCL molar ratio in deuterated DMSO (DMSO-d_6)

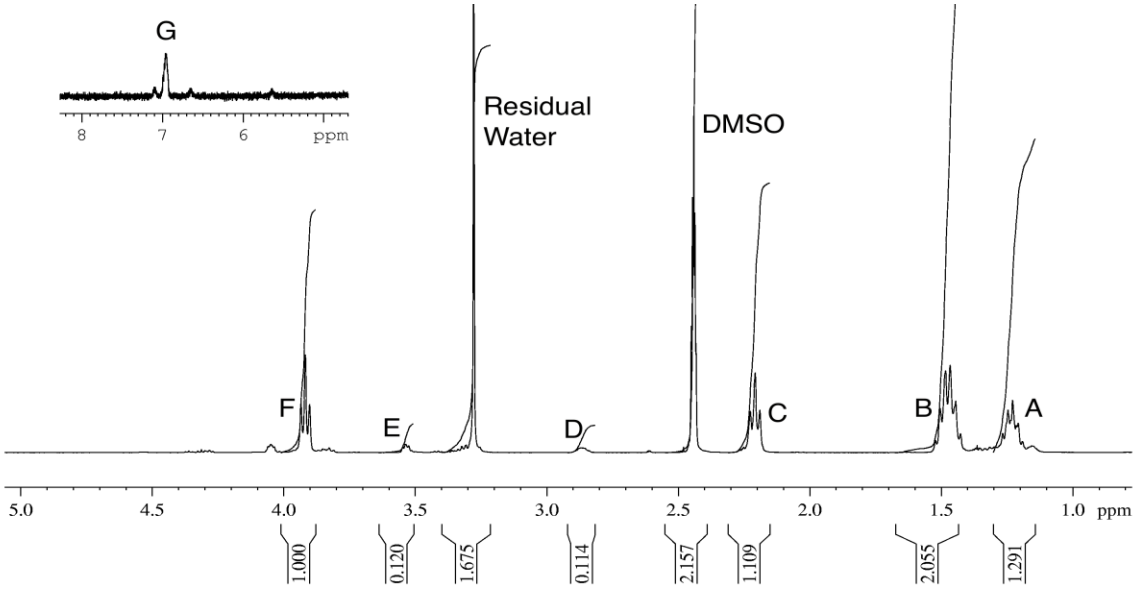

Figure 33. ^{1}H NMR spectrum of polyurethane sample with 1:2 HDI:PCL (hard to soft segment) molar ratio in deuterated DMSO (DMSO-d_6)

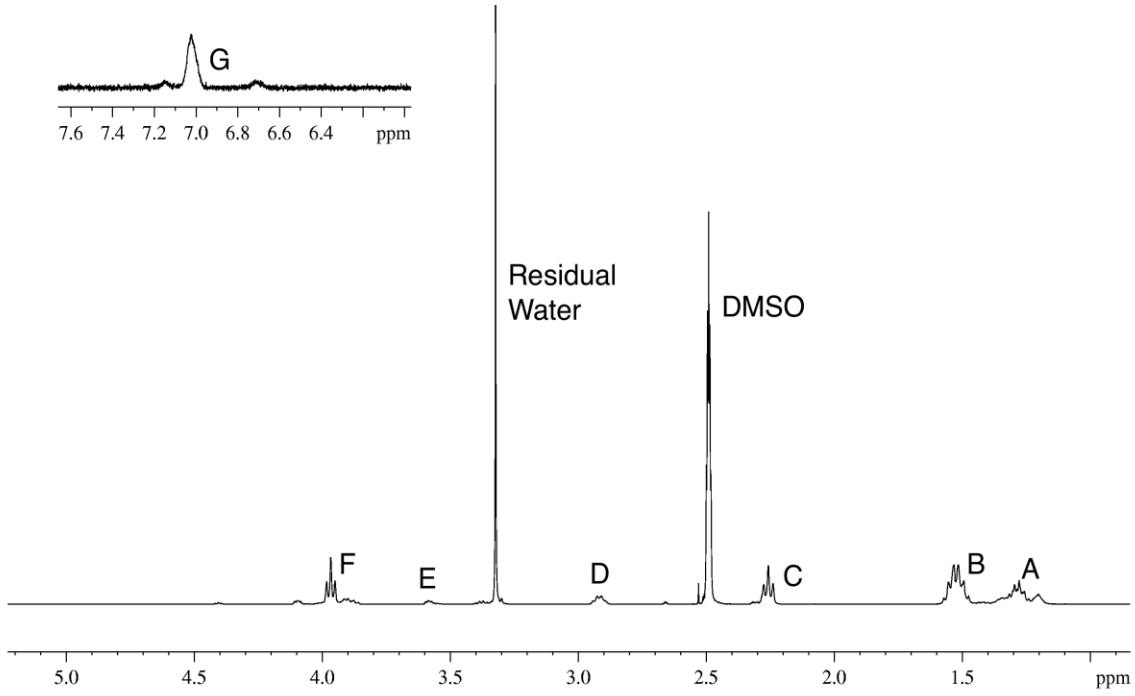

Figure 34. ^{1}H NMR spectrum of polyurethane sample with 2:1 HDI:PCL molar ratio in deuterated DMSO (DMSO-d_6)

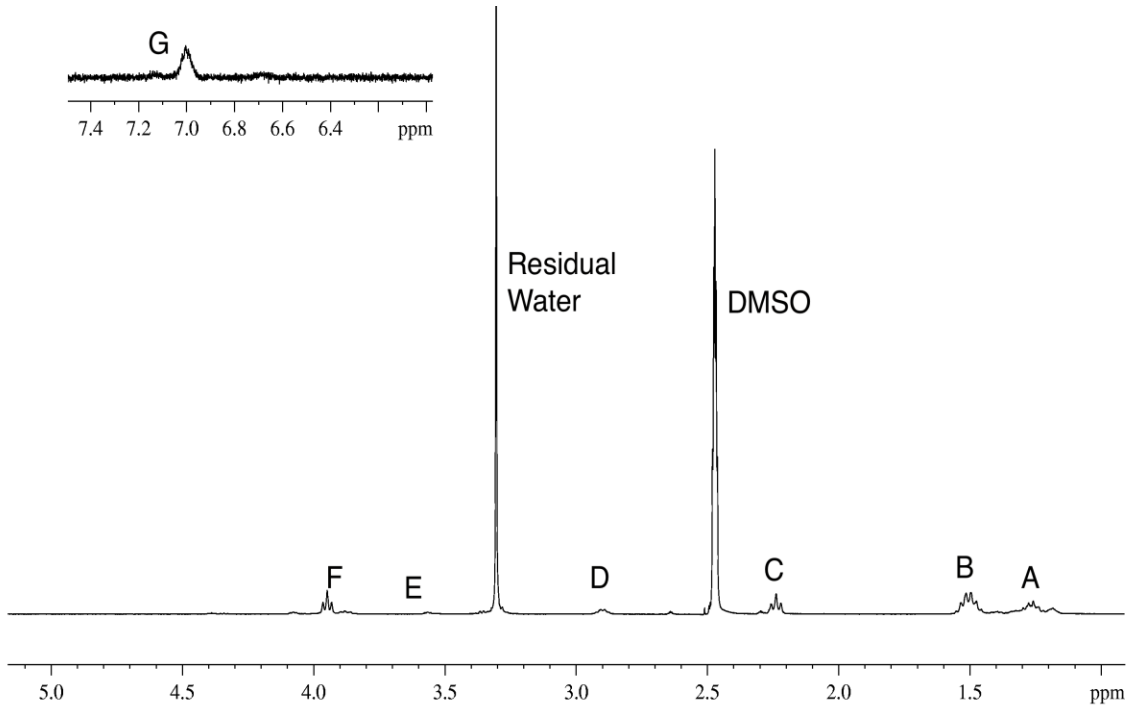

Figure 35. ^{1}H NMR spectrum of polyurethane sample with 4:1 HDI:PCL (hard to soft segment) molar ratio in deuterated DMSO (DMSO-d_6)

Appendix B: ASTM E8 Standard Test Methods for Mechanical Tension Testing of Materials

E8/E8M – 09

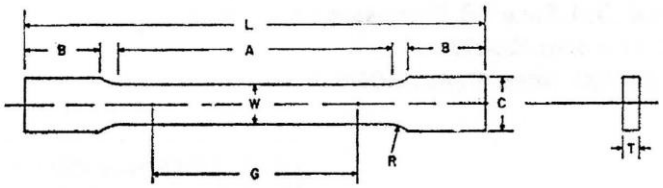

	Dimensions		
	Standard Specimens		Subsize Specimen
	Plate-Type, 40 mm [1.500 in.] Wide	Sheet-Type, 12.5 mm [0.500 in.] Wide	6 mm [0.250 in.] Wide
	mm [in.]	mm [in.]	mm [in.]
G—Gage length (Note 1 and Note 2)	200.0 ± 0.2 [8.00 ± 0.01]	50.0 ± 0.1 [2.000 ± 0.005]	25.0 ± 0.1 [1.000 ± 0.003]
W—Width (Note 3 and Note 4)	40.0 ± 2.0 [1.500 ± 0.125, -0.250]	12.5 ± 0.2 [0.500 ± 0.010]	6.0 ± 0.1 [0.250 ± 0.005]
T—Thickness (Note 5)		thickness of material	
R—Radius of fillet, min (Note 6)	25 [1]	12.5 [0.500]	6 [0.250]
L—Overall length, min (Note 2, Note 7, and Note 8)	450 [18]	200 [8]	100 [4]
A—Length of reduced section, min	225 [9]	57 [2.25]	32 [1.25]
B—Length of grip section, min (Note 9)	75 [3]	50 [2]	30 [1.25]
C—Width of grip section, approximate (Note 4 and Note 9)	50 [2]	20 [0.750]	10 [0.375]

NOTE 1—For the 40 mm [1.500 in.] wide specimen, punch marks for measuring elongation after fracture shall be made on the flat or on the edge of the specimen and within the reduced section. Either a set of nine or more punch marks 25 mm [1 in.] apart, or one or more pairs of punch marks 200 mm [8 in.] apart may be used.

NOTE 2—When elongation measurements of 40 mm [1.500 in.] wide specimens are not required, a minimum length of reduced section (*A*) of 75 mm [2.25 in.] may be used with all other dimensions similar to those of the plate-type specimen.

NOTE 3—For the three sizes of specimens, the ends of the reduced section shall not differ in width by more than 0.10, 0.05 or 0.02 mm [0.004, 0.002 or 0.001 in.], respectively. Also, there may be a gradual decrease in width from the ends to the center, but the width at each end shall not be more than 1 % larger than the width at the center.

NOTE 4—For each of the three sizes of specimens, narrower widths (*W* and *C*) may be used when necessary. In such cases the width of the reduced section should be as large as the width of the material being tested permits; however, unless stated specifically, the requirements for elongation in a product specification shall not apply when these narrower specimens are used.

NOTE 5—The dimension *T* is the thickness of the test specimen as provided for in the applicable material specifications. Minimum thickness of 40 mm [1.500 in.] wide specimens shall be 5 mm [0.188 in.]. Maximum thickness of 12.5 and 6 mm [0.500 and 0.250 in.] wide specimens shall be 19 and 6 mm [0.750 and 0.250 in.], respectively.

NOTE 6—For the 40 mm [1.500 in.] wide specimen, a 13 mm [0.500 in.] minimum radius at the ends of the reduced section is permitted for steel specimens under 690 MPa [100 000 psi] in tensile strength when a profile cutter is used to machine the reduced section.

NOTE 7—The dimension shown is suggested as a minimum. In determining the minimum length, the grips must not extend in to the transition section between Dimensions *A* and *B*, see Note 9.

NOTE 8—To aid in obtaining axial force application during testing of 6-mm [0.250-in.] wide specimens, the overall length should be as large as the material will permit, up to 200 mm [8.00 in.].

NOTE 9—It is desirable, if possible, to make the length of the grip section large enough to allow the specimen to extend into the grips a distance equal to two thirds or more of the length of the grips. If the thickness of 12.5 mm [0.500-in.] wide specimens is over 10 mm [0.375 in.], longer grips and correspondingly longer grip sections of the specimen may be necessary to prevent failure in the grip section.

NOTE 10—For the three sizes of specimens, the ends of the specimen shall be symmetrical in width with the center line of the reduced section within 2.5, 0.25 and 0.13 mm [0.10, 0.01 and 0.005 in.], respectively. However, for referee testing and when required by product specifications, the ends of the 12.5 mm [0.500 in.] wide specimen shall be symmetrical within 0.2 mm [0.01 in.].

NOTE 11—For each specimen type, the radii of all fillets shall be equal to each other within a tolerance of 1.25 mm [0.05 in.], and the centers of curvature of the two fillets at a particular end shall be located across from each other (on a line perpendicular to the centerline) within a tolerance of 0.2 mm [0.01 in.].

NOTE 12—Specimens with sides parallel throughout their length are permitted, except for referee testing, provided: *(a)* the above tolerances are used; *(b)* an adequate number of marks are provided for determination of elongation; and *(c)* when yield strength is determined, a suitable extensometer is used. If the fracture occurs at a distance of less than 2 W from the edge of the gripping device, the tensile properties determined may not be representative of the material. In acceptance testing, if the properties meet the minimum requirements specified, no further testing is required, but if they are less than the minimum requirements, discard the test and retest.

Figure 36. ASTM standards for E8 mechanical testing

Appendix C: Raw Experimental Data

Table 9. Compressive strengths and errors associated with pure, porous, and reinforced scaffolds

HDI:PCL molar ratio (hard to soft segment)	4:1	2:1	1:1	1:2	1:4
Pure Comp 1 (MPa)	19.61	19.61	5.02	2.28	2.17
Pure Comp 2 (MPa)	19.64	18.83	4.39	2.47	2.22
Pure Comp 3 (MPa)	19.64	17	5.44	2.39	2.06
Pure Compressive Error (+/-) (MPa)	0.017	1.340	0.528	0.095	0.373
%RSD (experimental error)	0.08	7.25	10.67	4.00	11.71
Porous Comp 1 (MPa)	0.83	0.61	0.36	0.14	0.12
Porous Comp 2 (MPa)	0.89	0.69	0.33	0.16	0.14
Porous Comp 3 (MPa)	0.97	0.75	0.3	0.15	0.144
Porous Compressive Error (+/-) (MPa)	0.070	0.070	0.030	0.010	0.012
%RSD (experimental error)	7.83	10.27	9.09	6.66	9.54
Reinforced Comp 1 (MPa)	1.75	1.11	0.57	0.23	0.18
Reinforced Comp 2 (MPa)	1.66	1.07	0.5	0.18	0.23
Reinforced Comp 3 (MPa)	1.50	1.29	0.58	0.22	0.20
Reinforced Compressive Error (+/-) (MPa)	0.127	0.117	0.044	0.026	0.025
%RSD (experimental error)	7.74	10.13	7.92	12.60	12.38

Table 10. Porosity measurements and calculations for both non-reinforced and reinforced samples

HDI:PCL molar ratio	**4:1**	**2:1**	**1:1**	**1:2**	**1:4**
Non-reinforced Porosity (%)	70.5	71.4	72.7	73.9	75.0
V1 (mL) - volume of ethanol	100	51	88	68	80
V2 (mL) - ethanol w/ scaffold	105	53	91	74	84
V3 (mL) - residual ethanol	88	46	80	51	68
Reinforced Porosity (%)	64.7	64.2	66.6	70.0	68.0
V1 (mL) - volume of ethanol	83	54	72	68	100
V2 (mL) - ethanol w/ scaffold	89	59	74	74	108
V3 (mL) - residual ethanol	72	45	68	54	83

REFERENCES

Al-Abdallah, W. (2012). Production of Biocellulose Nanofibers from Renewable Resources of Agricultural Residues. Ryerson University.

Albrektsson, T., and Johansson, C. (2001). Osteoinduction, osteoconduction and osseointegration. European Spine Journal *10*, 96–101.

Asefnejad, A., Khorasani, M.T., Behnamghader, A., Farsadzadeh, B., and Bonakdar, S. (2011). Manufacturing of biodegradable polyurethane scaffolds based on polycaprolactone using a phase separation method: physical properties and in vitro assay. International Journal of Nanomedicine *6*, 2375.

Asplund, J.O.B., Bowden, T., Mathisen, T., and Hilborn, J. (2007). Synthesis of highly elastic biodegradable poly (urethane urea). Biomacromolecules *8*, 905–911.

Bengtson, B., Feger, C., MacKnight, W.J., and Schneider, N.S. (1985). Thermal and mechanical properties of solution polymerized segmented polyurethanes with butadiene soft segments. Polymer *26*, 895–900.

Bovey, F.A., and Mirau, P.A. (1996). Nmr of Polymers (Academic Press).

Bruin, P., Veenstra, G.J., Nijenhuis, A.J., and Pennings, A.J. (1988). Design and synthesis of biodegradable poly(ester-urethane) elastomer networks composed of non-toxic building blocks. Die Makromolekulare Chemie, Rapid Communications *9*, 589–594.

Buffa, F., Abraham, G.A., Grady, B.P., and Resasco, D. (2007). Effect of nanotube functionalization on the properties of single-walled carbon nanotube/polyurethane composites. Journal of Polymer Science Part B: Polymer Physics *45*, 490–501.

Burstein, A.H., Reilly, D.T., Martens, M., and others (1976). Aging of bone tissue: mechanical properties. The Journal of Bone and Joint Surgery. American Volume *58*, 82.

Cao, X., Dong, H., and Li, C.M. (2007). New Nanocomposite Materials Reinforced with Flax Cellulose Nanocrystals in Waterborne Polyurethane. Biomacromolecules *8*, 899–904.

Cardy, R.H., and others (1979). Carcinogenicity and chronic toxicity of 2, 4-toluenediamine in F344 rats. Journal of the National Cancer Institute *62*, 1107.

Chan-Chan, L.H., Solis-Correa, R., Vargas-Coronado, R.F., Cervantes-Uc, J.M., Cauich-Rodríguez, J.V., Quintana, P., and Bartolo-Pérez, P. (2010). Degradation studies on segmented polyurethanes prepared with HMDI, PCL and different chain extenders. Acta Biomaterialia *6*, 2035–2044.

Co, M., and Dohme, M.S. (1899). The Merck manual of diagnosis and therapy (Merck).

Cohn, D., and Hotovely Salomon, A. (2005). Designing biodegradable multiblock PCL/PLA thermoplastic elastomers. Biomaterials *26*, 2297–2305.

Coury, A.J., Slaikeu, P.C., Cahalan, P.T., Stokes, K.B., and Hobot, C.M. (1988). Factors and Interactions Affecting the Performance of Polyurethane Elastomers in Medical Devices. J Biomater Appl *3*, 130–179.

Crawford, D.M., and Teets, A.R. (1997). The Effect of Strain on the Morphology and Mechanical Properties of Thermoplastic Polyurethane Elastomers (TPEs). (DTIC Document).

Cunningham, M., and Veenis, A. (2010) Tissue Regeneration: Bone Grafts and Nanofibre Scaffolding.

Dahman, Y. (2009). Nanostructured Biomaterials and Biocomposites from Bacterial Cellulose Nanofibers. Journal of Nanoscience and Nanotechnology *9*, 5105–5122.

Dahman, Y., Jayasuriya, K.E., and Kalis, M. (2010). Potential of biocellulose nanofibers production from agricultural renewable resources: preliminary study. Applied Biochemistry and Biotechnology *162*, 1647–1659.

Dahman, Y., and Sani, A. (2010). Optically Transparent Nanocomposite Reinforced With Modified Cellulose Nanofibers. Journal of Applied Polymer Science.

Den Dunnen, W.F.A., van der Lei, B., Schakenraad, J.M., Blaauw, E.H., Stokroos, I., Pennings, A.J., and Robinson, P.H. (1993). Long-term evaluation of nerve regeneration in a biodegradable nerve guide. Microsurgery *14*, 508–515.

Dvir, T., Timko, B.P., Kohane, D.S., and Langer, R. (2010). Nanotechnological strategies for engineering complex tissues. Nature Nanotechnology *6*, 13–22.

E28 Committee (2011). Test Methods for Tension Testing of Metallic Materials (ASTM International).

Fernández-d'Arlas, B., Khan, U., Rueda, L., Coleman, J.N., Mondragon, I., Corcuera, M.A., and Eceiza, A. (2011). Influence of hard segment content and nature on

polyurethane/multiwalled carbon nanotube composites. Composites Science and Technology *71*, 1030–1038.

Fernández-d'Arlas, B., Khan, U., Rueda, L., Martin, L., Ramos, J.A., Coleman, J.N., González, M.L., Valea, A., Mondragon, I., Corcuera, M.A., et al. (2012). Study of the mechanical, electrical and morphological properties of PU/MWCNT composites obtained by two different processing routes. Composites Science and Technology *72*, 235–242.

Fromstein, J.D., and Woodhouse, K.A. (2002). Elastomeric biodegradable polyurethane blends for soft tissue applications. Journal of Biomaterials Science, Polymer Edition *13*, 391–406.

Fujimoto, K.L., Guan, J., Oshima, H., Sakai, T., and Wagner, W.R. (2007). In vivo evaluation of a porous, elastic, biodegradable patch for reconstructive cardiac procedures. The Annals of Thoracic Surgery *83*, 648–654.

Gibson, L.J. (1985). The mechanical behaviour of cancellous bone. Journal of Biomechanics *18*, 317–328.

Girardi, F.P., and Bros, V. (2007). Worldwide orthopedic and spine market. Nucleus Arthroplasty Technology in Spinal Care: Fundamentals *1*,.

Goldstein, S.A. (1987). The mechanical properties of trabecular bone: dependence on anatomic location and function. Journal of Biomechanics *20*, 1055–1061.

Gorna, K., and Gogolewski, S. (2002a). Biodegradable polyurethanes for implants. II. In vitro degradation and calcification of materials from poly (ϵ-caprolactone)–poly (ethylene

oxide) diols and various chain extenders. Journal of Biomedical Materials Research *60*, 592–606.

Gorna, K., and Gogolewski, S. (2002b). In vitro degradation of novel medical biodegradable aliphatic polyurethanes based on ϵ-caprolactone and Pluronics® with various hydrophilicities. Polymer Degradation and Stability *75*, 113–122.

Gorna, K., and Gogolewski, S. (2003). Preparation, degradation, and calcification of biodegradable polyurethane foams for bone graft substitutes. Journal of Biomedical Materials Research Part A *67*, 813–827.

Gorna, K., and Gogolewski, S. (2006). Biodegradable porous polyurethane scaffolds for tissue repair and regeneration. Journal of Biomedical Materials Research Part A *79*, 128–138.

Gottlieb, H.E., Kotlyar, V., and Nudelman, A. (1997). NMR chemical shifts of common laboratory solvents as trace impurities. The Journal of Organic Chemistry *62*, 7512–7515.

Grad, S., Kupcsik, L., Gorna, K., Gogolewski, S., and Alini, M. (2003). The use of biodegradable polyurethane scaffolds for cartilage tissue engineering: potential and limitations. Biomaterials *24*, 5163–5171.

Gretzer, C., Gisselfält, K., Liljensten, E., Ryden, L., and Thomsen, P. (2003). Adhesion, apoptosis and cytokine release of human mononuclear cells cultured on degradable poly (urethane urea), polystyrene and titanium in vitro. Biomaterials *24*, 2843–2852.

De Groot, J.H., Kuijper, H.W., and Pennings, A.J. (1997a). A novel method for fabrication of biodegradable scaffolds with high compression moduli. Journal of Materials Science: Materials in Medicine *8*, 707–712.

De Groot, J.H., Nijenhuis, A.J., Bruin, P., Pennings, A.J., Veth, R.P.H., Klompmaker, J., and Jansen, H.W.B. (1990). Use of porous biodegradable polymer implants in meniscus reconstruction. 1) Preparation of porous biodegradable polyurethanes for the reconstruction of meniscus lesions. Colloid & Polymer Science *268*, 1073–1081.

De Groot, J.H., De Vrijer, R., Pennings, A.J., Klompmaker, J., Veth, R.P.H., and Jansen, H.W.B. (1996). Use of porous polyurethanes for meniscal reconstruction and meniscal prostheses. Biomaterials *17*, 163–173.

De Groot, J.H., De Vrijer, R., Wildeboer, B.S., Spaans, C.S., and Pennings, A.J. (1997b). New biomedical polyurethane ureas with high tear strengths. Polymer Bulletin *38*, 211–218.

Guan, J., Fujimoto, K.L., Sacks, M.S., and Wagner, W.R. (2005). Preparation and characterization of highly porous, biodegradable polyurethane scaffolds for soft tissue applications. Biomaterials *26*, 3961–3971.

Guan, J., Stankus, J.J., and Wagner, W.R. (2007). Biodegradable elastomeric scaffolds with basic fibroblast growth factor release. Journal of Controlled Release *120*, 70–78.

Guan, J., and Wagner, W.R. (2005). Synthesis, characterization and cytocompatibility of polyurethaneurea elastomers with designed elastase sensitivity. Biomacromolecules *6*, 2833–2842.

Guelcher, S.A. (2008). Biodegradable polyurethanes: synthesis and applications in regenerative medicine. Tissue Engineering Part B: Reviews *14*, 3–17.

Guelcher, S.A., Srinivasan, A., Dumas, J.E., Didier, J.E., McBride, S., and Hollinger, J.O. (2008). Synthesis, mechanical properties, biocompatibility, and biodegradation of polyurethane networks from lysine polyisocyanates. Biomaterials *29*, 1762–1775.

Gunatillake, P., Mayadunne, R., and Adhikari, R. (2006). Recent developments in biodegradable synthetic polymers. Biotechnology Annual Review *12*, 301–347.

Gunatillake, P.A., Adhikari, R., and others (2003). Biodegradable synthetic polymers for tissue engineering. Eur Cell Mater *5*, 1–16.

Harris, L.D., Kim, B.-S., and Mooney, D.J. (1998). Open pore biodegradable matrices formed with gas foaming. Journal of Biomedical Materials Research *42*, 396–402.

Hassan, M.K., Mauritz, K.A., Storey, R.F., and Wiggins, J.S. (2006). Biodegradable aliphatic thermoplastic polyurethane based on poly ($ărepsilon$-caprolactone) and L-lysine diisocyanate. Journal of Polymer Science Part A: Polymer Chemistry *44*, 2990–3000.

Heijkants, R., Van Calck, R.V., De Groot, J.H., Pennings, A.J., and Schouten, A.J. (2005a). Phase transitions in segmented polyesterurethane–DMSO–water systems. Journal of Polymer Science Part B: Polymer Physics *43*, 716–723.

Heijkants, R., van Calck, R.V., van Tienen, T.G., de Groot, J.H., Pennings, A.J., Buma, P., Veth, R.P.H., and Schouten, A.J. (2008). Polyurethane scaffold formation via a

combination of salt leaching and thermally induced phase separation. Journal of Biomedical Materials Research Part A *87*, 921–932.

Heijkants, R.G.J.C., Calck, R.V., Van Tienen, T.G., De Groot, J.H., Buma, P., Pennings, A.J., Veth, R.P., and Schouten, A.J. (2005b). Uncatalyzed synthesis, thermal and mechanical properties of polyurethanes based on poly ([epsilon]-caprolactone) and 1, 4-butane diisocyanate with uniform hard segment. Biomaterials *26*, 4219–4228.

Heijkants, R.G.J.C., Van Calck, R.V., De Groot, J.H., Pennings, A.J., Schouten, A.J., Van Tienen, T.G., Ramrattan, N., Buma, P., and Veth, R.P. (2004). Design, synthesis and properties of a degradable polyurethane scaffold for meniscus regeneration. Journal of Materials Science: Materials in Medicine *15*, 423–427.

Heijkants, R.G.J.C., Van Tienen, T.G., De Groot, J.H., Pennings, A.J., Buma, P., Veth, R.P., and Schouten, A.J. (2006). Preparation of a polyurethane scaffold for tissue engineering made by a combination of salt leaching and freeze-drying of dioxane. Journal of Materials Science *41*, 2423–2428.

Helenius, G., Bäckdahl, H., Bodin, A., Nannmark, U., Gatenholm, P., and Risberg, B. (2006). In vivo biocompatibility of bacterial cellulose. Journal of Biomedical Materials Research Part A *76A*, 431–438.

Hench, L.L., and Wilson, J. (1993). An introduction to bioceramics. World Scientific Pub Co Inc.

Holzapfel, G.A. (2001). Biomechanics of soft tissue. The Handbook of Materials Behavior Models *3*, 1049–1063.

Hood, M.A., Wang, B., Sands, J.M., La Scala, J.J., Beyer, F.L., and Li, C.Y. (2010). Morphology control of segmented polyurethanes by crystallization of hard and soft segments. Polymer *51*, 2191–2198.

Hou, Q., Grijpma, D.W., and Feijen, J. (2003). Porous polymeric structures for tissue engineering prepared by a coagulation, compression moulding and salt leaching technique. Biomaterials *24*, 1937–1947.

Huang, S.-L., and Lai, J.-Y. (1997). Structure-tensile properties of polyurethanes. European Polymer Journal *33*, 1563–1567.

Hubbe, M.A., Rojas, O.J., Lucia, L.A., and Sain, M. (2008). Cellulosic nanocomposites: a review. BioResources *3*, 929–980.

Hutmacher, D.W. (2000). Scaffolds in tissue engineering bone and cartilage. Biomaterials *21*, 2529–2543.

Jell, G., Verdejo, R., Safinia, L., Shaffer, M.S., Stevens, M.M., and Bismarck, A. (2008). Carbon nanotube-enhanced polyurethane scaffolds fabricated by thermally induced phase separation. J. Mater. Chem. *18*, 1865–1872.

Karageorgiou, V., and Kaplan, D. (2005). Porosity of 3D biomaterial scaffolds and osteogenesis. Biomaterials *26*, 5474–5491.

Kerin, A.J., Wisnom, M.R., and Adams, M.A. (1998). The compressive strength of articular cartilage. Proceedings of the Institution of Mechanical Engineers, Part H: Journal of Engineering in Medicine *212*, 273–280.

Khan, F., and Dahman, Y. (2012). A Novel Approach for the Utilization of Biocellulose Nanofibres in Polyurethane Nanocomposites for Potential Applications in Bone Tissue Implants. Designed Monomers & Polymers *15*, 1–29.

Kızıltay, A., Fernandez, A.M., Roman, J.S., Hasirci, V., and Hasirci, N. (2012). Lysine Based Poly(ester-urethane) Films for Tissue Engineering Applications. Journal of Biomaterials and Tissue Engineering *2*, 143–153.

Korley, L.S.T.J., Pate, B.D., Thomas, E.L., and Hammond, P.T. (2006). Effect of the degree of soft and hard segment ordering on the morphology and mechanical behavior of semicrystalline segmented polyurethanes. Polymer *47*, 3073–3082.

Lee, D.K., and Tsai, H.B. (2000). Properties of segmented polyurethanes derived from different diisocyanates. Journal of Applied Polymer Science *75*, 167–174.

Leong, K.F., Chua, C.K., Sudarmadji, N., and Yeong, W.Y. (2008). Engineering functionally graded tissue engineering scaffolds. Journal of the Mechanical Behavior of Biomedical Materials *1*, 140–152.

Liu, H., Zhang, L., Shi, P., Zou, Q., Zuo, Y., and Li, Y. (2010). Hydroxyapatite/polyurethane scaffold incorporated with drug-loaded ethyl cellulose microspheres for bone regeneration. Journal of Biomedical Materials Research Part B: Applied Biomaterials *95*, 36–46.

Marcovich, N.E., Auad, M.L., Bellesi, N.E., Nutt, S.R., and Aranguren, M.I. (2006). Cellulose micro/nanocrystals reinforced polyurethane. Journal of Materials Research *21*, 870–881.

MaRS (2009). Regenerative Medicine: Industry Briefing.

Martina, M., and Hutmacher, D.W. (2007). Biodegradable polymers applied in tissue engineering research: A review. Polymer International *56*, 145–157.

Märtson, M., Viljanto, J., Hurme, T., Laippala, P., and Saukko, P. (1999). Is cellulose sponge degradable or stable as implantation material? An in vivo subcutaneous study in the rat. Biomaterials *20*, 1989–1995.

Matheson, L.A., Santerre, J.P., and Labow, R.S. (2004). Changes in macrophage function and morphology due to biomedical polyurethane surfaces undergoing biodegradation. Journal of Cellular Physiology *199*, 8–19.

Meador, M.A.., Vivod, S.L., McCorkle, L., Quade, D., Sullivan, R.M., Ghosn, L.J., Clark, N., and Capadona, L.A. (2008). Reinforcing polymer cross-linked aerogels with carbon nanofibers. J. Mater. Chem. *18*, 1843–1852.

Mosekilde, L., and Mosekilde, L. (1986). Normal vertebral body size and compressive strength: relations to age and to vertebral and iliac trabecular bone compressive strength. Bone *7*, 207–212.

Oertel, G., and Abele, L. (1993). Polyurethane handbook (Hanser).

Pangarkar, N., and Hutmacher, D.W. (2003). Invention and Business Performance in the Tissue-Engineering Industry. Tissue Engineering *9*, 1313–1322.

Petrović, Z.S., Javni, I., and Divjaković, V. (1998). Structure and physical properties of segmented polyurethane elastomers containing chemical crosslinks in the hard segment. Journal of Polymer Science Part B: Polymer Physics *36*, 221–235.

Porter, J.R., Ruckh, T.T., and Popat, K.C. (2009). Bone tissue engineering: a review in bone biomimetics and drug delivery strategies. Biotechnology Progress *25*, 1539–1560.

Reichert, J.C., Wullschleger, M.E., Cipitria, A., Lienau, J., Cheng, T.K., Schütz, M.A., Duda, G.N., Nöth, U., Eulert, J., and Hutmacher, D.W. (2011). Custom-made composite scaffolds for segmental defect repair in long bones. International Orthopaedics *35*, 1229–1236.

Ryszkowska, J.L., Auguścik, M., Sheikh, A., and Boccaccini, A.R. (2010). Biodegradable polyurethane composite scaffolds containing Bioglass® for bone tissue engineering. Composites Science and Technology *70*, 1894–1908.

Saito, N., and Takaoka, K. (2003). New synthetic biodegradable polymers as BMP carriers for bone tissue engineering. Biomaterials *24*, 2287–2293.

Sánchez-Adsuar, M.S., Pastor-Blas, M.M., and Martín-Martínez, J.M. (1998). Properties of Polyurethane Elastomers with Different Hard/Soft Segment Ratio. The Journal of Adhesion *67*, 327–345.

Sánchez–Adsuar, M.S., Papon, E., and Villenave, J. (2000a). Influence of the prepolymerization on the properties of thermoplastic polyurethane elastomers. Part I. Prepolymer characterization. Journal of Applied Polymer Science *76*, 1596–1601.

Sánchez–Adsuar, M.S., Papon, E., and Villenave, J. (2000b). Influence of the prepolymerization on the properties of thermoplastic polyurethane elastomers. Part II. Relationship between the prepolymer and polyurethane properties. Journal of Applied Polymer Science *76*, 1602–1607.

Sani, A., and Dahman, Y. (2009). Improvements in the production of bacterial synthesized biocellulose nanofibres using different culture methods. Journal of Chemical Technology and Biotechnology *85*, 151–164.

Santerre, J.P., Woodhouse, K., Laroche, G., and Labow, R.S. (2005). Understanding the biodegradation of polyurethanes: From classical implants to tissue engineering materials. Biomaterials *26*, 7457–7470.

Schmidt-Nielsen, K. (1984). Scaling, why is animal size so important? (Cambridge Univ Pr).

Shikinami, Y., Matsusue, Y., and Nakamura, T. (2005). The complete process of bioresorption and bone replacement using devices made of forged composites of raw hydroxyapatite particles/poly l-lactide (Fu-HA/PLLA). Biomaterials *26*, 5542–5551.

Siepe, M., Giraud, M.N., Pavlovic, M., Receputo, C., Beyersdorf, F., Menasché, P., Carrel, T., and Tevaearai, H.T. (2006). Myoblast-seeded biodegradable scaffolds to prevent post–myocardial infarction evolution toward heart failure. The Journal of Thoracic and Cardiovascular Surgery *132*, 124–131.

Siró, I., and Plackett, D. (2010). Microfibrillated cellulose and new nanocomposite materials: a review. Cellulose *17*, 459–494.

Skarja, G.A., and Woodhouse, K.A. (1998). Synthesis and characterization of degradable polyurethane elastomers containing an amino acid-based chain extender. Journal of Biomaterials Science, Polymer Edition *9*, 271–295.

Skarja, G.A., and Woodhouse, K.A. (2000). Structure-property relationships of degradable polyurethane elastomers containing an amino acid-based chain extender. Journal of Applied Polymer Science *75*, 1522–1534.

Slivka, M.A., Leatherbury, N.C., Kieswetter, K., and Niederauer, G.G. (2001). Porous, Resorbable, Fiber-Reinforced Scaffolds Tailored for Articular Cartilage Repair. Tissue Engineering *7*, 767–780.

Spaans, C.J., Belgraver, V.W., Rienstra, O., De Groot, J.H., Veth, R.P.H., and Pennings, A.J. (2000). Solvent-free fabrication of micro-porous polyurethane amide and polyurethane-urea scaffolds for repair and replacement of the knee-joint meniscus. Biomaterials *21*, 2453–2460.

Spaans, C.J., Dekens, F.G., Groot, J.H.D.E., and Pennings, A.J. (2003). Biomedical polyurethane, its preparation and use.

Spaans, C.J., De Groot, J.H., Dekens, F.G., and Pennings, A.J. (1998). High molecular weight polyurethanes and a polyurethane urea based on 1, 4-butanediisocyanate. Polymer Bulletin *41*, 131–138.

Stankus, J.J., Guan, J., Fujimoto, K., and Wagner, W.R. (2006). Microintegrating smooth muscle cells into a biodegradable, elastomeric fiber matrix. Biomaterials *27*, 735–744.

Storey, R.F., Wiggins, J.S., Mauritz, K.A., and Puckett, A.D. (1993). Bioabsorbable composites. II: Nontoxic, L-lysine-based poly (ester-urethane) matrix composites. Polymer Composites *14*, 17–25.

Sumi, M., Chokki, Y., Nakai, Y., Nakabayashi, M., and Kanzawa, T. (1964). Studies on the structure of polyurethane elastomers. I. NMR spectra of the model compounds and some linear polyurethanes. Die Makromolekulare Chemie *78*, 146–156.

Szycher, M., Siciliano, A.A., and others (1991). An assessment of 2, 4 TDA formation from Surgitek polyurethane foam under simulated physiological conditions. Journal of Biomaterials Applications *5*, 323.

Tatai, L., Moore, T.G., Adhikari, R., Malherbe, F., Jayasekara, R., Griffiths, I., and Gunatillake, P.A. (2007). Thermoplastic biodegradable polyurethanes: The effect of chain extender structure on properties and in-vitro degradation. Biomaterials *28*, 5407–5417.

Tienen, T.G., Heijkants, R., Buma, P., De Groot, J.H., Pennings, A.J., and Veth, R.P.H. (2003). A porous polymer scaffold for meniscal lesion repair–A study in dogs. Biomaterials *24*, 2541–2548.

Trivieri, L. New Ways to Maintain Healthy Bones.

Tseng, S., and Tang, S.C. (2007). Synthesis and characterization of the novel transfection reagent poly (amino ester glycol urethane). Biomacromolecules *8*, 50–58.

Turner, C.H., Wang, T., and Burr, D.B. (2001). Shear strength and fatigue properties of human cortical bone determined from pure shear tests. Calcified Tissue International *69*, 373–378.

Wan, Y.Z., Luo, H., He, F., Liang, H., Huang, Y., and Li, X.L. (2009). Mechanical, moisture absorption, and biodegradation behaviours of bacterial cellulose fibre-reinforced starch biocomposites. Composites Science and Technology *69*, 1212–1217.

Xu, H.H.K., Quinn, J.B., Takagi, S., Chow, L.C., and Eichmiller, F.C. (2001). Strong and macroporous calcium phosphate cement: effects of porosity and fiber reinforcement on mechanical properties. Journal of Biomedical Materials Research *57*, 457–466.

Xu, M., Macknight, W.J., Chen, C.H.Y., and Thomas, E.L. (1983). Structure and morphology of segmented polyurethanes: 1. Influence of incompatability on hard-segment sequence length. Polymer *24*, 1327–1332.

Yang, S., Leong, K.F., Du, Z., and Chua, C.K. (2001). The design of scaffolds for use in tissue engineering. Part I. Traditional factors. Tissue Engineering *7*, 679–689.

Yilgor, I., Yilgor, E., Guler, I.G., Ward, T.C., and Wilkes, G.L. (2006). FTIR investigation of the influence of diisocyanate symmetry on the morphology development in model segmented polyurethanes. Polymer *47*, 4105–4114.

Zaborowska, M., Bodin, A., Bäckdahl, H., Popp, J., Goldstein, A., and Gatenholm, P. (2010). Microporous bacterial cellulose as a potential scaffold for bone regeneration. Acta Biomaterialia *6*, 2540–2547.

Zhang, J.Y., Beckman, E.J., Piesco, N.P., and Agarwal, S. (2000). A new peptide-based urethane polymer: synthesis, biodegradation, and potential to support cell growth in vitro. Biomaterials *21*, 1247–1258.